Journal of Pharmaceutical Analysis 10 (2020) 397–413

Contents lists available at ScienceDirect

Journal of Pharmaceutical Analysis

journal homepage: www.elsevier.com/locate/jpa

Review paper

Recent progress in the molecular imaging of therapeutic monoclonal antibodies

Kaifeng He, Su Zeng, Linghui Qian*

Institute of Drug Metabolism and Pharmaceutical Analysis, Zhejiang Province Key Laboratory of Anti-Cancer Drug Research, College of Pharmaceutical Sciences, Zhejiang University, Hangzhou, 310058, China

ARTICLE INFO

Article history:
Received 1 February 2020
Received in revised form
1 June 2020
Accepted 21 July 2020
Available online 8 August 2020

Keywords:
Therapeutic monoclonal antibodies
Molecular structure
Biological function
Molecular imaging

ABSTRACT

Therapeutic monoclonal antibodies have become one of the central components of the healthcare system and continuous efforts are made to bring innovative antibody therapeutics to patients in need. It is equally critical to acquire sufficient knowledge of their molecular structure and biological functions to ensure the efficacy and safety by incorporating new detection approaches since new challenges like individual differences and resistance are presented. Conventional techniques for determining antibody disposition including plasma drug concentration measurements using LC-MS or ELISA, and tissue distribution using immunohistochemistry and immunofluorescence are now complemented with molecular imaging modalities like positron emission tomography and near-infrared fluorescence imaging to obtain more dynamic information, while methods for characterization of antibody's interaction with the target antigen as well as visualization of its cellular and intercellular behavior are still under development. Recent progress in detecting therapeutic antibodies, in particular, the development of methods suitable for illustrating the molecular dynamics, is described here.

1. Introduction

Monoclonal antibodies (mAbs) have attracted increasing attention as the most rapidly growing drug class towards diseases such as cancer, autoimmune disorders, and chronic inflammatory diseases due to their high specificity and affinity for targeted antigens [1–3]. Soon after Köhler et al. [4] fused B cells with myeloma cells to facilitate the efficient production of mAbs in 1975, the world's first mAb drug OKT3 (Muromonab-CD3) was approved by the US Food and Drug Administration (FDA) in 1985, followed by the launch of the first fully human mAb, Adalimumab, attributing to the breakthrough of phage display technology in 2002 [5]. Therapeutic mAbs entered a rapid development stage since then, with a total number of 64 approved mAbs by the US FDA in 2018 [3] and 5 novel antibody therapeutics have been granted the first approval as of November 2019 with 79 more undergoing evaluations in late-stage clinical studies [6]. With improvements in genetic engineering and conjugation strategies, therapeutic mAbs have expanded from full-length immunoglobulin G (IgG) containing double heavy and light chains to derivatives like single-chain antibody (ScFv), nanobody, affibody, bispecific antibody, etc. as well as immunoconjugates where the antibody is linked with payloads like radioisotopes or drugs (antibody-drug conjugates, ADCs), making them more complex in the structure than small-molecule drugs. In addition, the binding activity, selectivity, immunogenicity, and stability are also critical for their efficacy [7]. Therefore, accurate detection and analysis of their molecular structure and biological functions is crucial in guaranteeing the safety and efficacy of therapeutic mAbs during their development, manufacturing and clinical applications. This review will describe these approaches with a focus on the progress in the molecular imaging of mAbs to illustrate their biological functions.

2. Analysis of molecular structure

2.1. Primary and higher-order structure

The molecular mass of mAb can be indicative of its primary structure, and mass spectrometry (MS) alone [8,9] or coupled with efficient separation methods like liquid chromatography (LC; including reverse-phase [10,11], size-exclusion [12,13], and ion-exchange chromatography [14]) and capillary electrophoresis (CE)

Peer review under responsibility of Xi'an Jiaotong University.

* Corresponding author.
E-mail address: lhqian@zju.edu.cn (L. Qian).

https://doi.org/10.1016/j.jpha.2020.07.006

[15] can therefore be used to identify the primary structure of mAbs. To further identify the peptide sequence, the amide bond between a specific amino acid sequence is cleaved by chemical or enzymatic methods, followed by analysis with MS [16].

Since the function of mAb highly relies on its higher-order structure (HOS), different structural characterization methods are applied. Nuclear magnetic resonance (NMR) and X-ray crystallography can provide structural information at atomic level resolution, but lengthy sample preparation (like isotope labeling or crystallization)/data acquisition periods and instrument availability limit their application in the industry. Fourier transform infrared spectroscopy (FT-IR) [17] and far-UV (≤240 nm) circular dichroism (CD) spectroscopy [18] are commonly used to determine its secondary structure (i.e., α-helix, β-sheet, and random coils) in a nondestructive and quantitative manner. The tertiary structure can be analyzed using near-UV (260–320 nm) CD spectroscopy [19], but the complicated buffer matrices may interfere with the detection and the CD signal is the sum of the whole mAb without information for which part of the protein contributes to the signal change. Alternatively, the tertiary and quaternary conformation can be investigated by some MS-based methods (e.g., native MS, ion-mobility MS, and hydrogen-deuterium exchange MS (HDX-MS)) [20], and the HDX-MS can also pinpoint where the conformation changes occur. However, MS is expensive and has low throughput, and high-throughput protein conformational array is recently in progress [21].

2.2. Heterogeneity

Unlike small molecules, mAbs not only have large size, but also undergo post-translational modifications (PTMs), degradation, aggregation and other chemical modifications during preparation or storage, leaving their structures highly heterogeneous. Among them, *N*-glycosylation is commonly found in mAbs and is crucial for their structural and functional properties, which will influence the stability, pharmacokinetics, immunogenicity, antibody-dependent cellular cytotoxicity (ADCC), and complement-dependent cytotoxicity (CDC) [22,23]. For example, high mannose type reduces plasma half-life, increases immunogenicity and ADCC [24]. To monitor and control the uniformity of mAbs is thus important for drug quality control.

Most of currently approved therapeutic mAbs belong to the IgG isotype, with the same basic Y-shape structure built from double heavy chains (50 kDa each) and double light chains (25 kDa each; Fig. 1A), of which the Fc (Fragment crystallizable) has a highly conserved *N*-glycosylation site on 297 asparagine (Asn297, Fig. 1A) [25–27]. The most common oligosaccharides found in current antibody therapeutics are shown in Fig. 1B [28]. The glycosylation of mAbs is closely related to the genetic engineering, expression system (yeast, mammalian, and plant) and the incubation condition. Controlling glycosylation can bias the effect of the Fc-related functions of therapeutic antibodies [29,30], so glycol-engineering technologies are also being developed to control glycoforms (Fig. 1B, right) [28,31]. Very recently, Weiss's group [32] engineered Chinese hamster ovary (CHO) cells with synthetic genetic circuits to rationally tune *N*-glycosylation of a stably expressed IgG under small-molecule inducible promoters. With the help of a bio-orthogonal small-molecule inducer, they achieved stable expression of the glycosyltransferase genes at tunable levels, allowing for a wide range of galactosylated and fucosylated species not easily accessible before. Apart from Asn297, *N*-glycosylation sites are also present on the Fab (Fragment of antigen binding) [25,26] and some antibodies have been found to have *O*-glycosylation modifications [33,34]. The absence of these oligosaccharides has no effect on the binding ability but has a profound effect on mAb effector functions [1], requiring thorough analysis of glycosylation of mAb drugs.

LC-MS is commonly used for characterizing the glycosylation of mAbs [35,36]. In order to improve the sensitivity of MS (especially with MALDI-TOF-MS), it can be performed with the peptide fragments or with sugar chain by enzyme- or chemistry-assisted release. However, there are still some problems, such as low recovery and enrichment of glycopeptide, low throughput of sample processing, and poor method sensitivity, waiting to be addressed with more efficient and reliable detection methods. CE is another convenient method to analyze glycosylation. For example, CE-SDS can be used to rapidly analyze the glycan occupancy and the number of glycosylation sites. The separation between glycosylated and non-glycosylated proteins is largely due to the fact that glycans do not bind SDS. Hence, the glycoprotein always migrates more slowly than its non-glycosylated counterpart [37]. To further identify glycan structures, MS is used to complement CE separations for the characterization of mAb variants [38,39].

3. Assessment of biological functions

Around half of currently approved antibody drugs are indicated for use in oncology, and an approximately similar number of antibodies are approved for the treatment of autoimmune and chronic inflammatory diseases [2]. On one hand, treatments targeting cancer and those treating autoimmunity seek opposite effects on the immune system—in cancer, to enhance immune responses against tumors; in autoimmunity, to promote immune suppression and curb inflammation—but both types of immunotherapy may work on the same immune pathways. Therefore, autoimmune diseases may benefit from the success of cancer immunotherapies, and techniques involved in the analysis of mAbs can also allow each to shed light on the other. On the other hand, though therapeutic mAs achieve remarkable clinical success and offer the possibility to treat tumors in a targeted fashion with reduced severe side effects, the responses of different patients vary [40–42]. Moreover, a significant increase in immune-related adverse events has emerged during cancer immunotherapies [43]. Unfortunately, the underlying mechanism is complicated and has not been fully elucidated yet. To this end, how mAbs act in vivo is to be better illustrated in urgency.

Taking cancer therapy as an example, according to the trajectory of mAb in vivo (Fig. 2) [1,2], factors affect its pharmacokinetics (PK) [44], interaction towards target antigen and subsequent cellular performance or intercellular immune response may contribute to the therapeutic outcome (Table 1) [40], and methods aiming to study these processes are described here.

3.1. Pharmacokinetics

Maintaining appropriate levels of mAbs ensures sufficient contact with antigens (e.g., the driving force for diffusion into the tumor) and the subtherapeutic concentrations of mAbs is proposed to cause the inefficacy or acquired resistance [45]. Also, some mAb drugs have immunogenicity and will stimulate the body to produce antibodies against them, called anti-drug antibody (ADA), to increase their clearance [46]. Therefore, monitoring mAbs in vivo is pivotal for the best therapeutic outcome.

3.1.1. Blood concentration

Usually PK studies are performed by administering the mAb followed by harvesting blood at pre-determined time points. After pretreatment and digestion, quantitative MS analysis is carried out [47]. Another conventional method for determining serum mAb concentrations is immunoassay including the enzyme-linked immunosorbent assay (ELISA) [48] and electrochemiluminescence immunoassay (ECLIA) [49,50]; however, they may suffer from

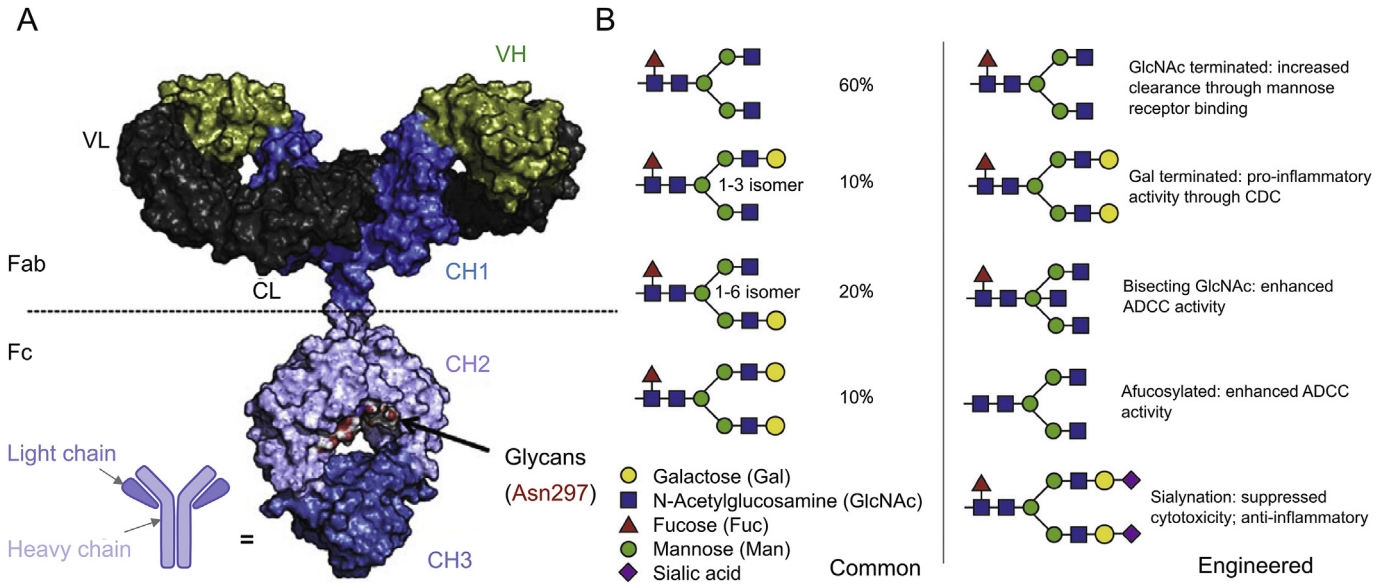

Fig. 1. (A) General structure of therapeutic monoclonal antibodies (IgG-type antibodies) [27]. (B) Therapeutic antibodies are glycosylated through the ubiquitous asparagine residue (Asn297) found in the Fc region. The most common oligosaccharides found in current therapeutic antibody products are shown (left). Several engineered oligosaccharides and the resulting impact on functions are shown (right) [28]. The figures were reproduced with permission from Refs. [27,28], respectively.

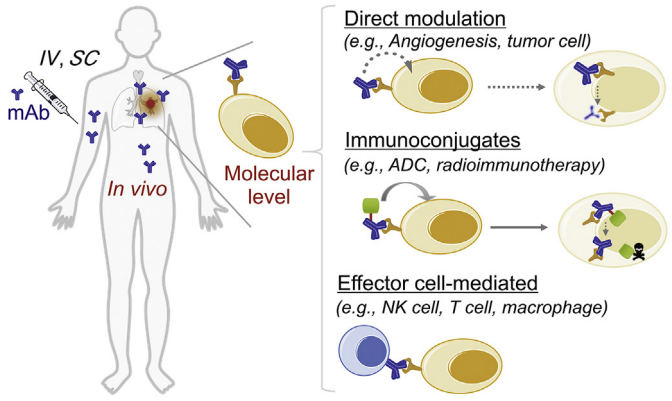

Fig. 2. Monoclonal antibody-based cancer therapeutic strategies.

lower precision (about 10% of relative standard deviation in repeatability) and robustness for quantification purposes [11].

Electrochemical-based biosensors quantify the antibody concentration by measuring the current or the impedance through various electrochemical analytical methods. They provide simple, cost-effective, and accurate measurements [51]. To gain comprehensive information from the same serum sample, Plaxco's group [52] designed a wash-free, electrochemical method for quantitative detection of multiple antibodies in unprocessed blood serum. The sensor mainly consists of a polypeptide epitope for the recognition of mAb and an electrode-bound, redox-reporter-modified DNA strand (Fig. 3A). Upon binding with mAb, the redox reporter will collide with the electrode and decrease electron transfer, causing a drop in peak current (Fig. 3B). The sensor can therefore simultaneously measure concentrations of multiple antibodies in a single sample with high sensitivity and specificity (Fig. 3C).

Surface plasmon resonance (SPR) biosensor has the obvious advantages of directly detecting and measuring serum antibodies in minutes; avoiding the long incubation, separation, washing or detection steps; and reducing complexity and variability [53]. Recently, Gobbi's group [54] developed a method to measure mAbs based on SPR. The apparatus has six flow channels which can immobilize up to six ligands; then the flow channels can be rotated 90° so that up to six serum samples can be flowed in parallel (Fig. 4A). They adopted this approach to measure serum concentrations of infliximab (IFX), an antibody against tumor necrosis factor α (TNFα), and antibodies towards IFX (ATI), measuring drug and antidrug antibodies simultaneously (Fig. 4B/C).

Though powerful, assays described so far are either semi-quantitative or require sophisticated devices. Bioluminescence does not require external excitation, avoiding background signals and light scattering during detection, making detection in complex matrices relatively straightforward. Merkx's group [55] developed a bioluminescent platform (LUMABS) that allows mAb detection directly in blood plasma. Binding of an antibody to the epitope

Table 1
Possible reasons for lack of therapeutic efficacy with mAbs [40].

Property	Possible reasons for lack of therapeutic efficacy
Pharmacokinetics	mAb stability, half-life and immunogenicity
Penetrance and concentration at targeted site	Vascular permeability, tumor interstitial pressure, micoenvironment, mAb size and affinity
Antigen occupancy	mAb-to-antigen concentration, antigen saturation/heterogeneity/mutation/expression downregulation and ineffective modulation of antigen function
Signaling pathway abrogation	Signaling pathway not relevant for tumor growth, compensatory or promiscuity of signaling pathways
Payload delivery and release	Inadequate concentration in target sites and drug resistance
Immune effector function	mAb isotype, FcγR polymorphism, immune escape/suppression, and complement inhibition

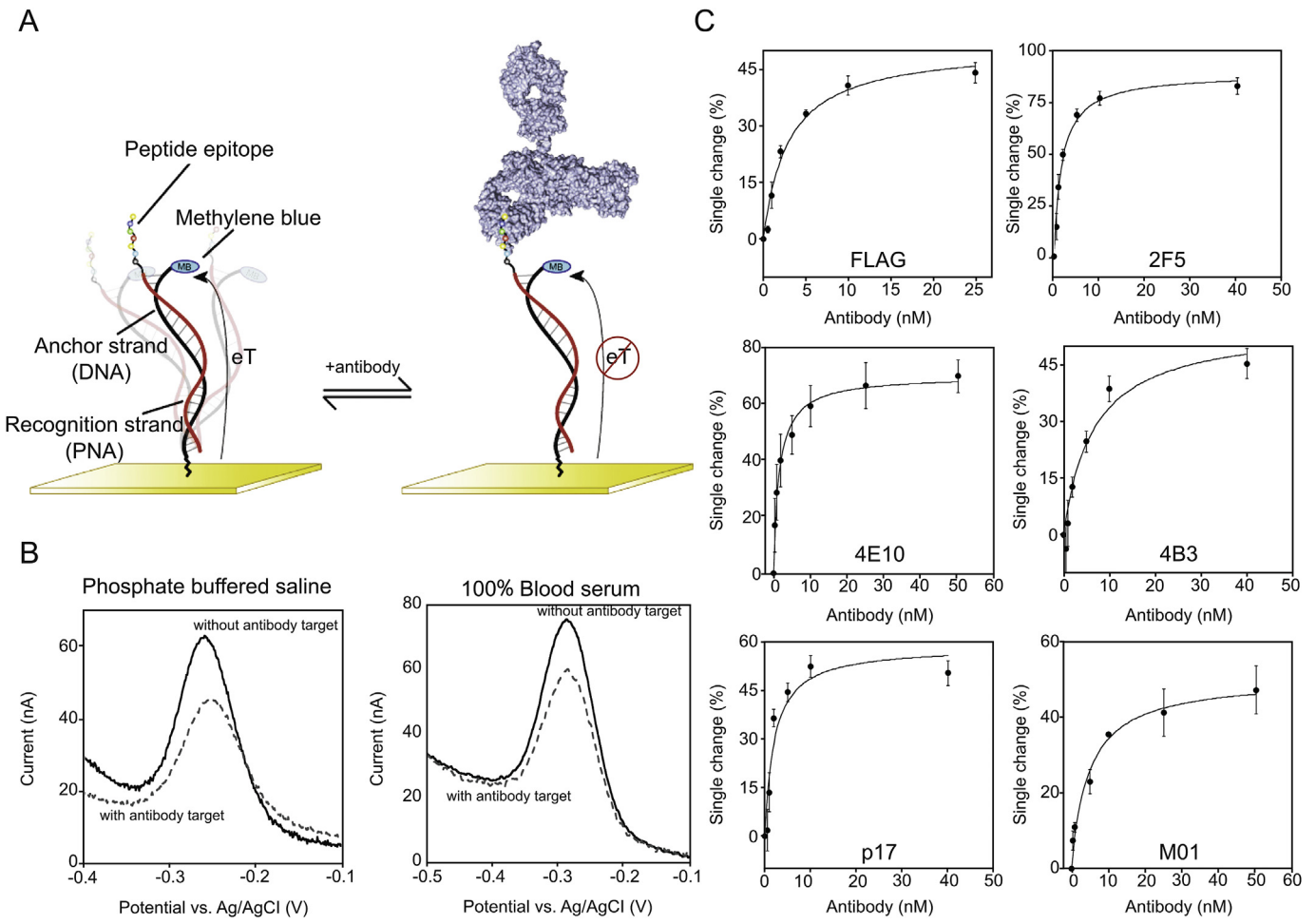

Fig. 3. (A) Design of the electrochemical sensor. (B) Binding of mAbs can be measured as a decrease in the peak current. (C) Quantitative detection of six antibodies against contiguous epitopes. The figure was reproduced with permission from Ref. [52].

results in a great decrease in the bioluminescence resonance energy transfer (BRET) efficiency which can be detected directly in blood plasma even at low pM concentrations of antibody. By simple exchange of the antibody-binding epitope sequences, LUMABS allows one to detect any desired antibody quickly.

3.1.2. Biodistribution

One of the most essential steps in the clinical evaluation of a potential mAb is the ratio for antibody uptake in the tumor versus normal tissues, since the enrichment of mAbs within the tumor is the prerequisite for successful tumor killing while the distribution within normal tissues is crucial for predicting toxicity. Biopsy is the commonly available choice. For instance, Hummon's group [56] developed a methodology that enables evaluation of therapeutic antibody distribution in tissues using MALDI-MSI. They used an on-tissue reduction and alkylation strategy to break disulfide bonds to generate smaller fragments suitable for direct analysis by MALDI-MSI. This label-free approach will be useful for visualizing the heterogeneous distribution of mAb drugs in tissues and tumors. However, biopsy has several limitations, such as sampling error and heterogeneity in target expression [57,58]. Additionally, a single time-point value may be insufficient due to the dynamic uptake. Therefore, direct in vivo imaging is highly desirable to track how the drug distributes inside the body.

3.1.2.1. Positron emission tomography (PET). PET is a nuclear imaging technique used to map biological processes in living creatures following the administration of radiolabeled tracers [59,60]. In vivo PET with radiolabeled mAb can help to study the kinetics of mAb delivery and localization in both animals and humans [61]. Cetuximab competitively targeting the ligand-binding site of epidermal growth factor receptor (EGFR) was the first mAb approved by the FDA for the treatment of EGFR-expressing, metastatic colorectal carcinoma [62]. As shown in Fig. 5A, whole-animal PET shows that uptake of ^{64}Cu-labeled cetuximab increases over time in EGFR-positive tumors but is relatively low in EGFR-negative tumors [63]. Coupled with computed tomography (CT), whole-body PET images indicating the biodistribution of antibodies in a patient can also be obtained (Fig. 5B) [64]. In particular, PET using radiolabeled antibodies also enables visualizing the location of potential cancers in vivo, well-known as Immuno-PET [65,66]. Conventional methods to radiolabel proteins with metal isotopes like ^{64}Cu, ^{68}Ga and ^{89}Zr require time-consuming procedures involving protein functionalization with a chelate, isolation, and subsequent radiolabeling and purification. To this end, Holland's group developed a fast, light-induced protein radiolabeling method under mild conditions with novel metal-ion-binding chelates derived from aryl azide groups. This one-pot photochemical conjugation and radiolabeling of mAbs can be achieved within 20 min [67]. Recent advances in bioconjugation technology also enable site-specific

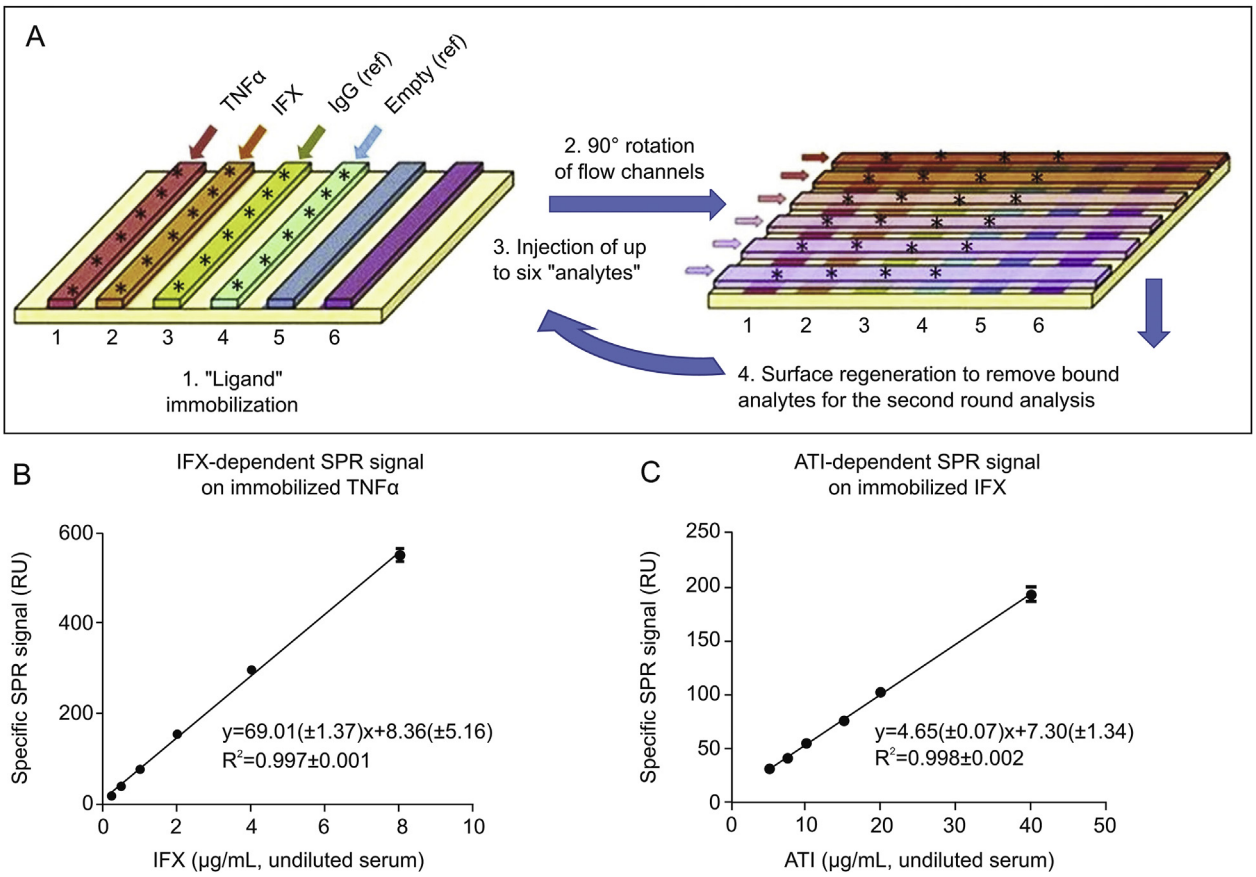

Fig. 4. (A) Scheme of the SPR-based assay for simultaneous determination of up to six serum samples. Linearity between (B) IFX or (C) ATI concentration and specific SPR signal. The figure was reproduced with permission from Ref. [54].

modification to generate well-defined constructs with superior properties and to allow better use of PET imaging towards mAbs [68]. Among natural amino acids, cysteine is preferred to lysine for selective protein modification due to its higher nucleophilicity, lower abundance and relatively specific and well-defined locations within mAbs (full-length IgGs typically contain 32 cysteine residues that can form 12 intrachain and 4 interchain disulfide bridges). However, any attempt to label cysteine residues must first overcome their disulfide cross-linkages without interfering with the function of the antibodies [69]. To circumvent this issue, either bifunctional construct that is capable of attaching a cargo to the mAb while also re-bridging the interchain (rarely been applied to radionuclide imaging yet) or genetic incorporation of engineered cysteines is employed. Another site-selective attachment method towards native IgGs relies on the two conserved glycosylation sites (Asn297). Either chemical or enzyme-mediated modification at these sites will not compromise antigen affinity as they are distal to the Fab region, producing more homogeneous and well-defined radioimmuno conjugates, and may also improve mAb in vivo performance [70]. Moreover, traceless tagging methods are also introduced, by which the modification upon mAbs can be eliminated after entering cells, to release the native form of mAbs [71]. Meanwhile, long-term tracking is also desirable to better match antibody circulation half-life in vivo. To extend the monitoring time with PET, Tarantal's group investigated the feasibility of lengthen ^{89}Zr-PET imaging using the highly sensitive primate miniEXPLORER PET system. Satisfactory image quality was obtained even at 30 days post injection, representing approximately 9-fold half-lives of ^{89}Zr to identify the activity of anti-gD IgG in different organs like liver, kidneys, and bone joints (Fig. 6) [72].

3.1.2.2. Near-infrared (NIR) fluorescence imaging. Though PET is highly sensitive with unlimited depth penetration, the high expense of the equipment and concerns of its radiation hazard limit its broad applicability for imaging [73,74]. Fluorescence-based imaging excels at high resolution, capable of dynamic imaging, low cost and convenient portability, based on which NIR fluorescence imaging is considered as a convenient and safe alternative for pharmacokinetic characterization of mAbs at the subcellular to tissue level as well as for disease diagnosis and intraoperative imaging. Moreover, dyes with different excitation/emission wavelengths can be used together for multichannel imaging [75]. Nimotuzumab is a humanized anti-EGFR antibody that has been approved in many countries for the treatment of EGFR-positive cancers. Bernhard et al. prepared an NIR fluorescent dye-labeled immunoconjugate, IRDye800CW-nimotuzumab, and evaluated its binding affinity, selectivity and stability (Figs. 7A–C) before measuring in vivo tumor uptake by NIR fluorescent imaging (Fig. 7D). In mice bearing EGFR-positive xenografts, IRDye800CW-nimotuzumab uptake peaked at 4 days post injection and slowly decreased thereafter with high levels of accumulation still observed at 28 days post injection [76]. Fluorescence imaging is unique in that each fluorophore emits its own characteristic spectral wavelength, thus permitting depiction of multiple targets simultaneously. Multiplexed use of differently colored NIR fluorophores to label several mAbs in the same subject can depict single lesion with increased accuracy, since the combination of several independent signals helps to reduce the false-positive results.

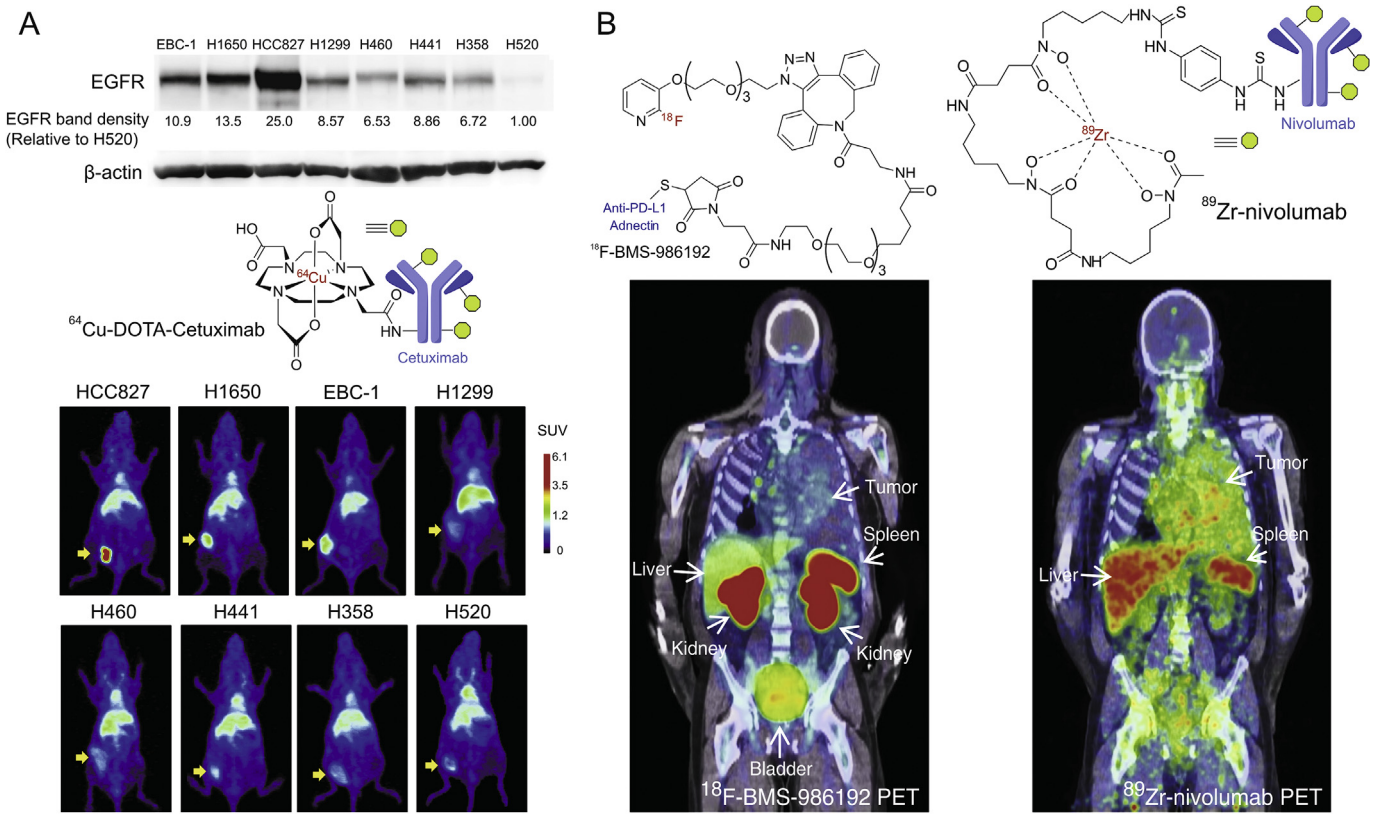

Fig. 5. (A) EGFR expression in eight non-small cell lung cancer (NSCLC) cell lines (up). Representative ^{64}Cu-DOTA-cetuximab PET images in mice xenograft models with NSCLC tumors containing varying EGFR expression levels at 48 h. Arrows indicate the location of tumors (down) [63]. (B) PET-CT of patient with tumor PD-L1 expression < 1%: ^{18}F-BMS-986192 PET (214.62 MBq, 1 h p.i.) demonstrates low tumor tracer uptake. ^{89}Zr-labeled Nivolumab PET (37.27 MBq, 160 h p.i.) demonstrates heterogeneous tracer uptake in the tumor [64]. The figures were reproduced with permission from Refs. [63,64], respectively.

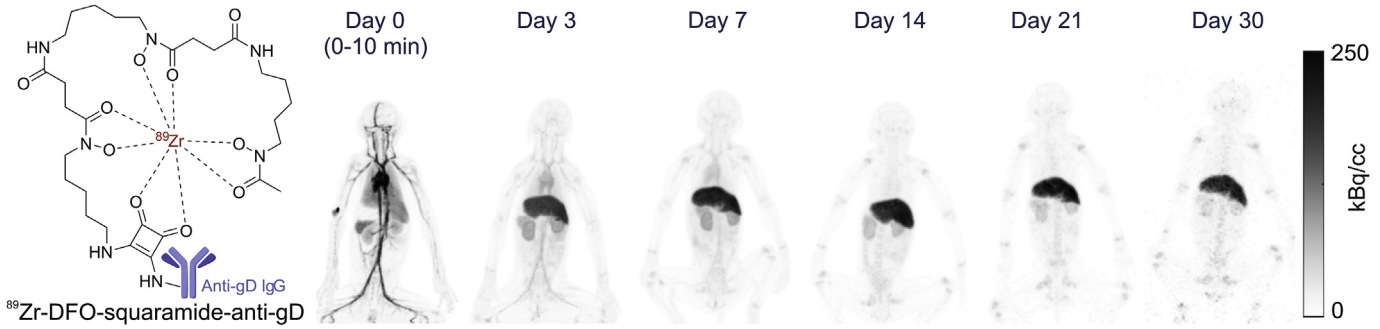

Fig. 6. Maximum intensity projection images at each time point for one of the rhesus monkeys in the ^{89}Zr-DFO-squaramide-anti-gD group. The figure was reproduced with permission from Ref. [72].

Multicolor imaging can also detect molecularly heterogeneous lesions in naturally occurring tumors over time (Fig. 8) [77–80]. This offers the ability to gain insights into multiple dimensions of the molecular milieu whereas conventional monochromatic imaging can only characterize a single molecular profile per imaging session. Real-time multicolor image-guided surgery was then performed in vivo to demonstrate that this technology could be used intraoperatively to differentiate different tumor types based on their multicolor fluorescence [81]. Similarly, when combined with the nuclear tracers (for PET) to the same fluorophore-labeled mAb, it is applicable to seamlessly carry out whole body imaging to determine the extent of diseases, followed by immediate fluorescence-guided surgical intervention [82].

3.2. Antibody-antigen interaction

One of the key distinguishing attributes of mAbs is their affinity for the target antigen, which is determined by the variable region/complementarity-determining region (CDR). Upon binding to the antigen, mAbs may act as the agonist or antagonist/blockage to modulate cell membrane receptors directly, or may recruit effector cells (especially cells responsible for immune response) to change the cell fate. When conjugated with other reagents like drugs or radionuclides, more efficient cell death can be achieved. Assessment of antibody-antigen interaction is therefore important for understanding the efficacy and toxicity of mAb or immunoconjugate treatment [83]. In vitro binding affinity of mAbs can be

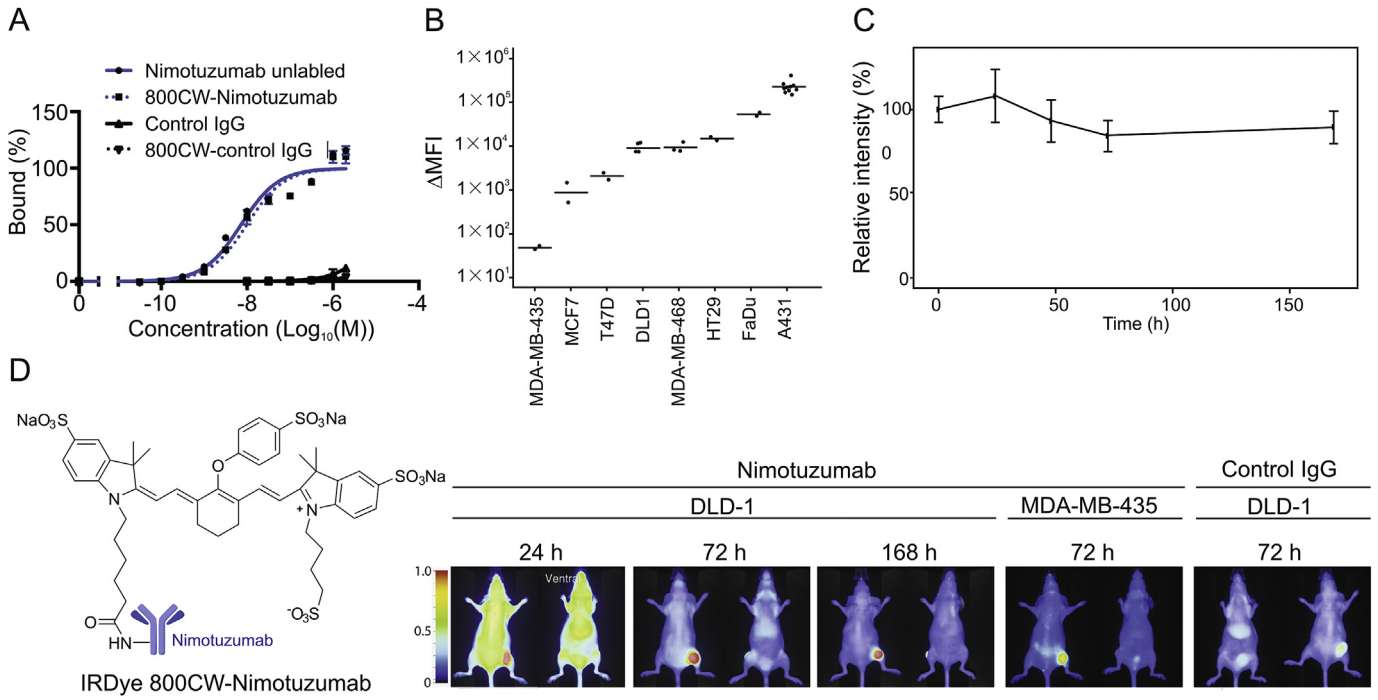

Fig. 7. (A) Titration curves of nimotuzumab, IRDye800CWnimotuzumab, and control IgG against DLD-1 cells showing percent bound against antibody concentration. (B) Nimotuzumab binding to cell lines expressing various levels of EGFR. (C) IRDye800CW-nimotuzumab stability was assayed in mouse serum at 37 °C over seven days. (D) Biodistribution analysis of IRDye800CW-nimotuzumab in mice bearing DLD-1 and MDA-MB-435 xenografts. Control IgG was injected into mice bearing DLD-1 xenografts. The figure was reproduced with permission from Ref. [76].

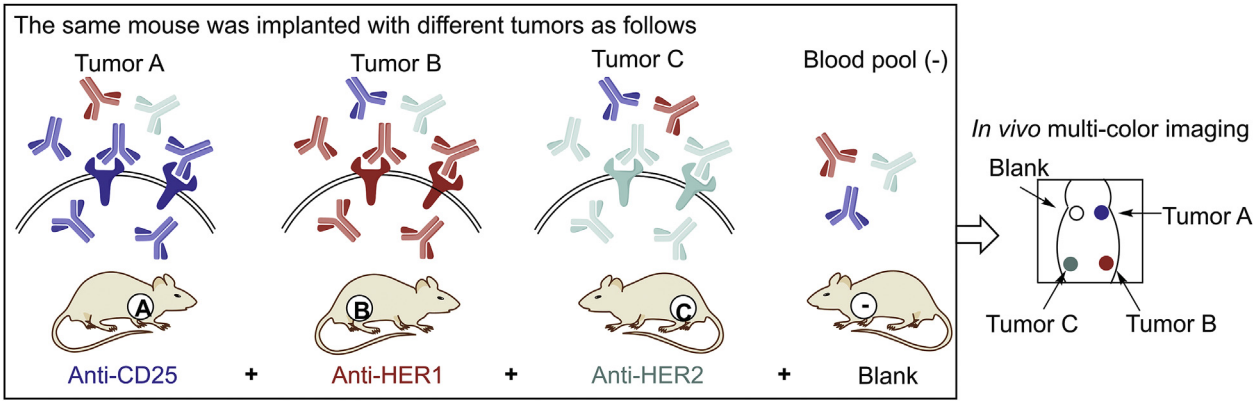

Fig. 8. Multi-color imaging targeting CD25, HER1, and HER2, using Alexa700-, Cy5-, and Cy7-labeled respective specific antibodies [79].

detected by methods as described for serum mAb concentrations including ELISA [84] and SPR assay [85,86], so they will not be specified here. Very recently, Yao's group [87] reported a sensor based on photonic crystal hydrogels (PCHs), which is capable of naked-eye detection of antibody-antigen interaction with high sensitivity, providing inspiration for detecting the interaction with advanced materials. Besides, new assays suitable for direct evaluation of the antigen engagement in living cells will be highlighted here.

Ryu's group presented a single-molecule diffusional-mobility-shift assay (smDIMSA) to analyze the interaction between cetuximab and EGFR on the membrane of living cells based on the finding that ligand-receptor interactions decrease the diffusional mobility of membrane receptors (Fig. 9A). This assay directly measured the interaction on a single living cell seeded on an inexpensive glass surface, thus greatly reducing experimental labor and cost. This technique enables quantitative analysis of the dissociation constant and the cooperativity of antibody interactions with EGFR and its mutants (Fig. 9B–D) [88]. To be noted, it remains a puzzle how the soluble region can affect the diffusivity of a membrane protein, so investigations of the underlying mechanism may be needed before its application to other mAb-receptor interactions.

Alternatively, atomic force microscopy (AFM) is a versatile technique for probing the biomechanical properties of interactions between biomolecules and their receptors on the surface of living cells with nanoscale spatial resolution. Shan's group [89] characterized the mechanical changes of living cells following cetuximab treatment by AFM to explore the single molecular interaction forces between cetuximab and EGFR on the cell surface (Fig. 10A/B),

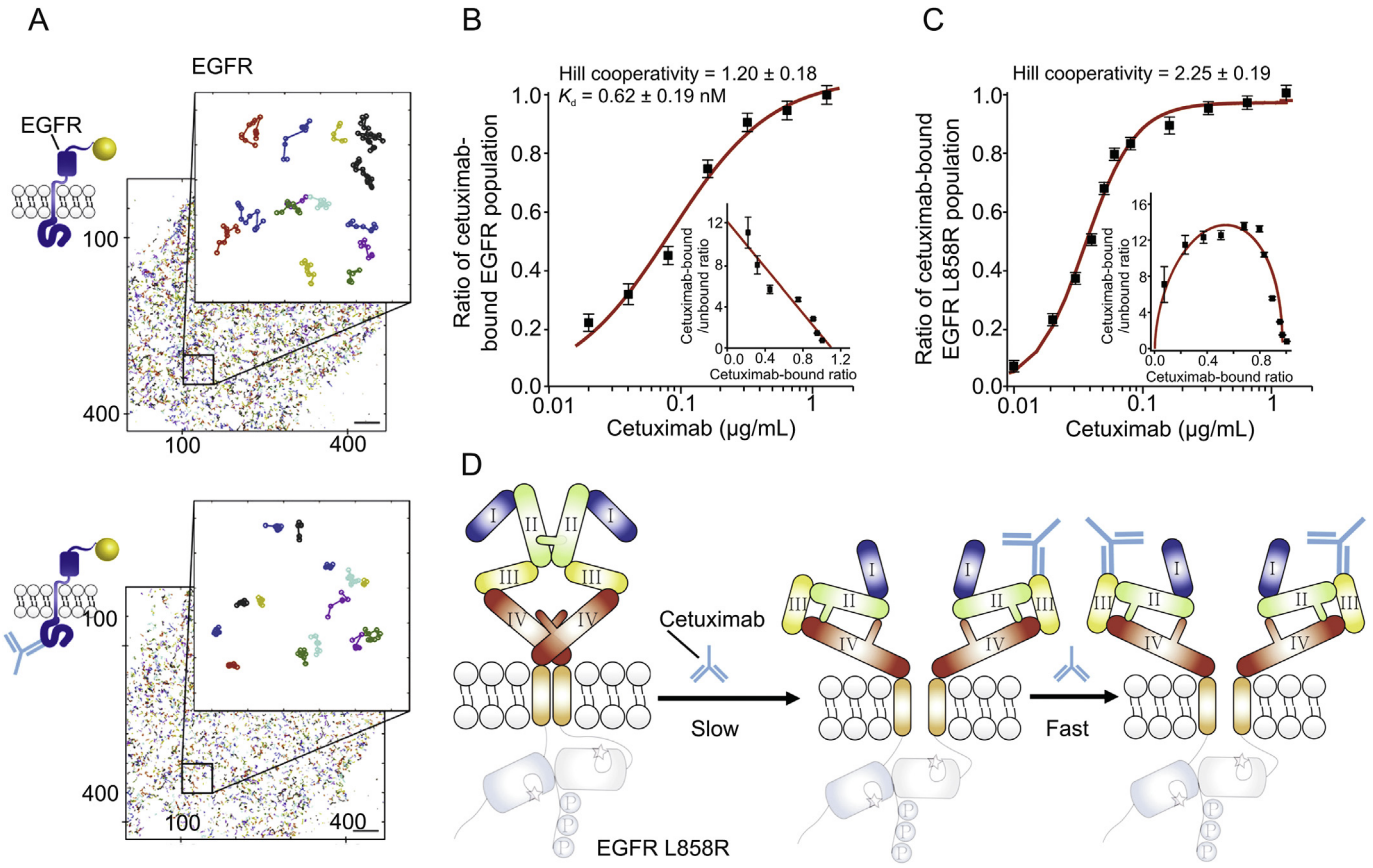

Fig. 9. (A) Map of accumulated EGFR trajectories acquired for about 1 min before (up) and after cetuximab treatment (after 3 min; down) in a single COS7 cell. (B-C) Dissociation constant and cooperativity measurement for the interaction of cetuximab with (B) wild-type EGFR and (C) its mutant (L858R) on a COS7 cell membrane. The insets show Scatchard plots to evaluate the interaction cooperativity. (D) Proposed model for the molecular mechanism of the positive cooperativity of cetuximab binding to EGFR L858R. The figure was reproduced with permission from Ref. [88].

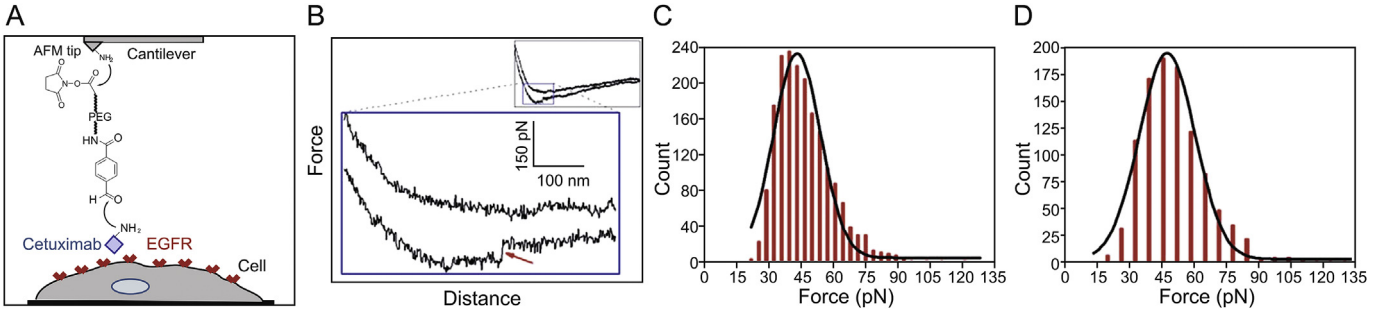

Fig. 10. (A) Scheme of experimental procedures. (B) A typical force-distance cycle of the specific interaction between cetuximab and cell membrane EGFR. (C) Histogram of cetuximab-EGFR binding forces. (D) Histogram of EGF-EGFR binding forces (n > 1000). The figure was reproduced with permission from Ref. [89].

suggesting the binding probability of cetuximab-EGFR was stronger than that of EGF-EGFR (Fig. 10C/D). Though powerful in binding affinity determination, the tip functionalization is quite complicated, requiring sophisticated skills to ensure accurate results and therefore limiting their wider applications.

In consideration of the fact that the in vivo assessment of antigen occupancy of mAbs is greatly limited by current technologies, Cao's group [90] developed a BRET-based system that leverages the large signal to noise ratio and stringent energy donor-acceptor distance dependency to measure antibody-antigen occupancy in a highly selective and temporal fashion (Fig. 11A). This versatile and minimally invasive system enables longitudinal monitoring of the in vivo antibody-antigen (e.g., cetuximab-EGFR) interaction in a tumor xenograft model over several days (Fig. 11B–D). This proof-of-concept study represents an extended use of BRET-based strategies towards antigen engagement; however, since pre-engineering of the receptor with luciferase is needed to achieve BRET, it may not be ideal for the determination of endogenous receptor occupancy towards mAbs from clinical samples.

3.3. Cellular performance

As depicted in Fig. 2, after binding to the target antigen, mAbs may undergo internalization or recruitment of the effector cells to execute the cancer cell killing. It is therefore in high demand to monitor these dynamic processes in real time with living cells for a

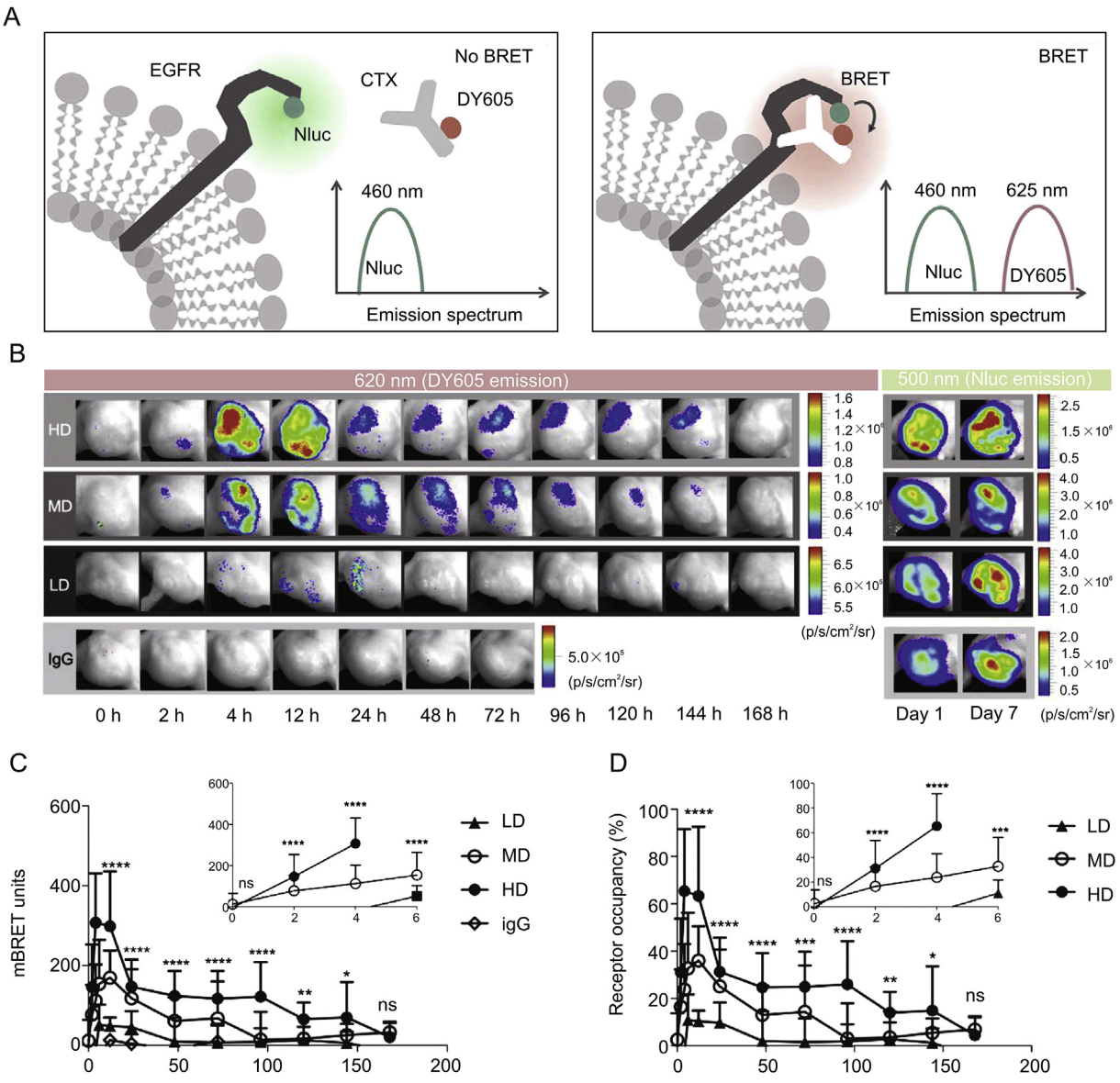

Fig. 11. (A) Schematic of the NanoLuc-EGFR/DY605-Cetuximab BRET System. NanoLuc (a 19-kDa luciferase) was fused to the N terminus of the EGFR extracellular domain to generate the BRET donor moiety. A fluorescent dye, DY605, was covalently appended onto cetuximab to generate the BRET acceptor moiety. (B-D) DY605-Cetuximab/NanoLuc-EGFR interaction measurement in vivo. (B) BRET images of mice that received 50 mg/kg (HD)/8.5 mg/kg (MD)/1.0 mg/kg (LD) of DY605-cetuximab or 1.9 mg/kg of control DY605-IgG. (C) Quantified NanoLuc-EGFR/DY605-cetuximab binding according to BRET ratios. (D) Quantified receptor occupancy in living mice. The figure was reproduced with permission from Ref. [90].

comprehensive understanding of how mAbs function.

Conventional "always-on" antibody-conjugated probes, such as gadolinium, radioisotopes and NIR fluorescent dyes as mentioned above, can provide direct tracking of mAb in vivo, while they suffer from high non-specific background signals in real-time imaging. Among them, fluorescence-based probes have the advantage that their signal is potentially switchable depending on local conditions (such as environment change or enzyme trigger) and are now commonly used to visualize cellular processes. Nevertheless, only a few activatable fluorescence probes exist for no-wash imaging of mAbs to study its biological performance, and we will review these probes here to inspire the development of more novel strategies.

3.3.1. Fluorescence activated through cellular internalization and degradation

As demonstrated in Fig. 12, most of the currently available "turn-on" strategies take advantages of the receptor-mediated endocytosis of mAbs followed by degradation in lysosomes to restore the fluorescence, such as activatable probes adopting fluorescence resonance energy transfer (FRET, Fig. 12A) [91,92]. However, in the strategy of FRET, multiple fluorescent and quenching molecules are labeled in one antibody, in which the labeling ratio and distance between the fluorophore and quencher are difficult to control while it will interfere with the final quenching efficiency. Hence conjugation with the same molecule will be preferred.

In addition to acting as a central organelle of proteolysis, lysosome can help to turn on certain fluorophores with its acidic pH (pH = 5–6; Fig. 12B). Trastuzumab, an antibody targeting the human epidermal growth factor receptor type 2 (HER2), is internalized via the endosomal-lysosomal degradation pathway after binding to HER2. Based on this, Urano et al. developed acidic pH-activatable boron-dipyrromethene (BODIPY) probes to

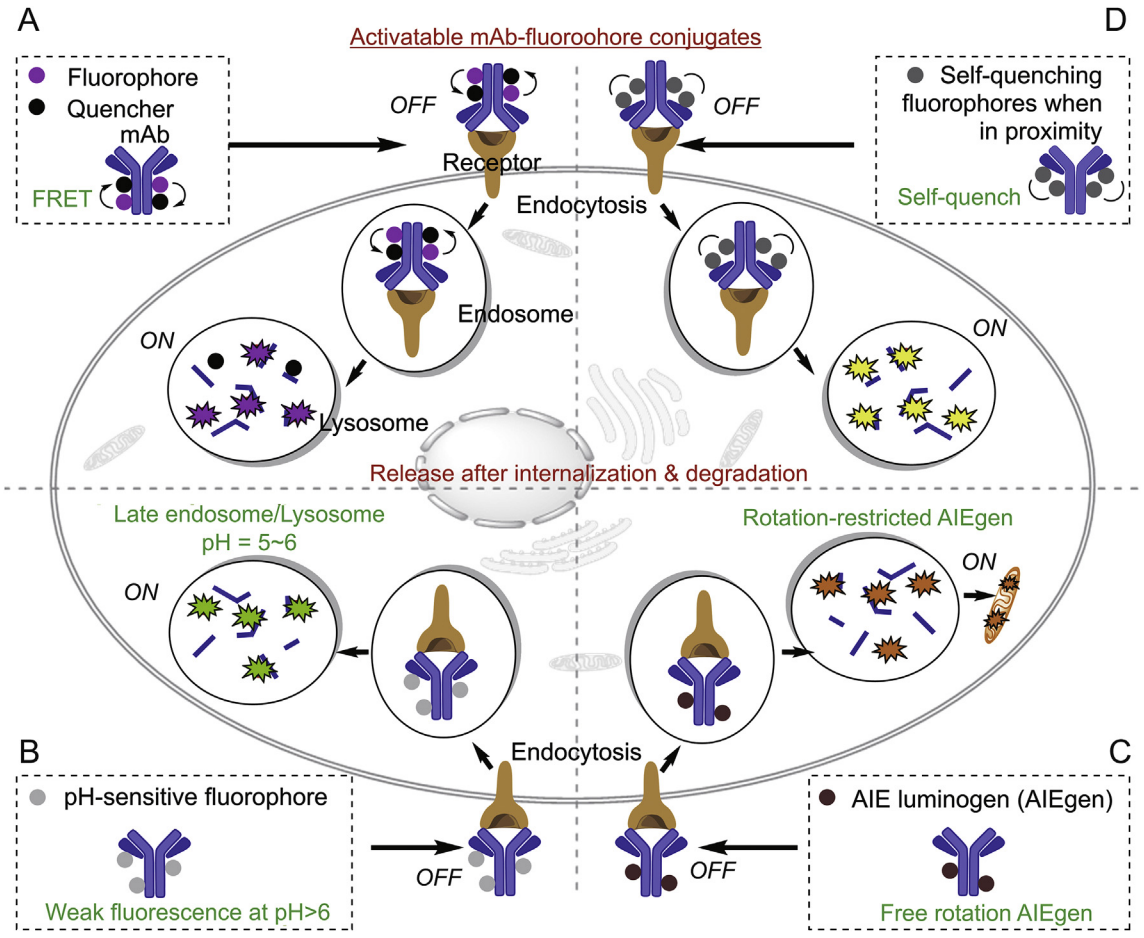

Fig. 12. A summary of available activatable mAb-fluorophore conjugates using (A) FRET, (B) acidic pH-sensitivity, (C) AIE, or (D) self-quenching strategies to study the cellular performance of mAbs based on receptor-mediated antibody internalization and degradation.

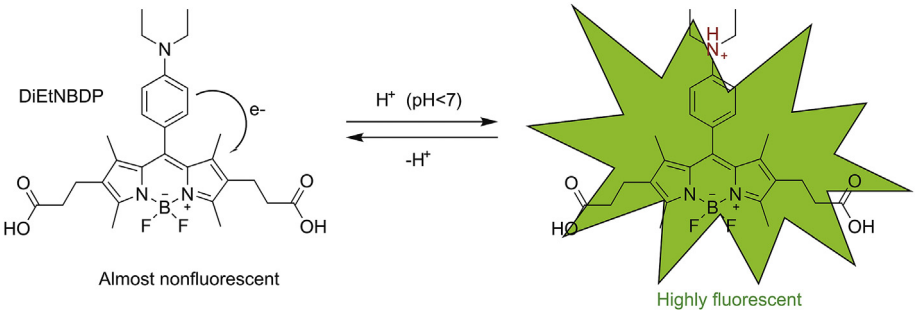

Fig. 13. Design of the reversible and acidic pH-induced fluorescence activation of BODIPY probe, DiEtNBDP [93].

label trastuzumab (Fig. 13). The resulting conjugate (almost nonfluorescent at neutral pH outside the cell or in the cytosol, and highly fluorescent at acidic pH in the lysosome) allowed no-wash monitoring of mAb internalization in viable lung cancer cells with high signal to background contrast [93]. NIR pH-activatable fluorophores were also developed with potential for in vivo imaging [94].

Recently, aggregation-induced emission (AIE) luminogens (AIEgens) have attracted intense research attention. They offer weak fluorescence when molecularly dissolved in good solvents. However, their emissions are greatly amplified in the aggregated state or in a confined environment owing to the restriction of intramolecular motion (RIM) [95–97]. In combination of AIE feature and lysosome degradation of mAb-receptor complex after internalization, Tang's group developed a new antibody-AIEgen conjugate with "turn-on" fluorescence (Fig. 12C). With the cetuximab connected to AIEgen (CSPP-NHS), due to the free rotation, the whole conjugate (mAb-CSPP) showed almost no fluorescence (Fig. 14A) [98]. Only when the conjugate entered cancer cells overexpressing EGFR through endocytosis and translocated into the lysosome for hydrolysis to leave the free AIEgens accumulated in the lysosome, could it become highly emissive (Fig. 14B/C). Excitingly, due to the aggregation potency, released AIEgens will not diffuse like other small-molecule dyes, minimizing false-positive signals. With a more comprehensive understanding of the emission behaviors of AIEgens, more AIEgens will be available for this strategy [99,100].

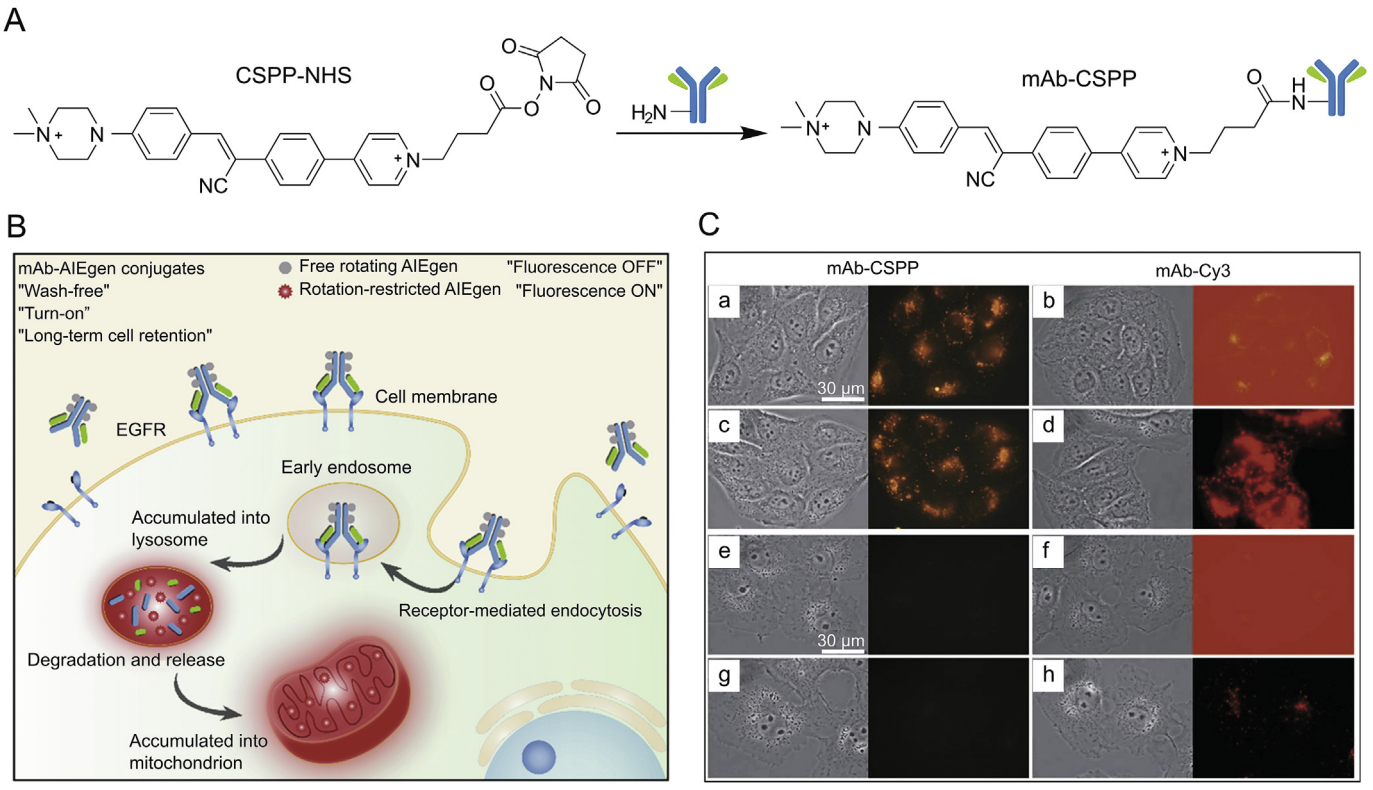

Fig. 14. (A) Preparation of the mAb-AIEgens conjugate. (B) Schematic representation of the "turn-on" process of mAb-AIEgen conjugates after internalization and catabolism in EGFR overexpressing cells. (C) Live-cell fluorescence images of (a–d) HCC827 cancer cells (EGFR-positive) and (e–h) COS-7 normal cells (EGFR-negative) incubated with cetuximab-CSPP and cetuximab-Cy3 conjugates for 12 h. Images were taken (a, b, e and f) without washing or (c, d, g and h) after washing. The figure was reproduced with permission from Ref. [98].

In contrast to AIE, certain dyes have the self-quenching potency when two or more of the same fluorophores are in such proximity that the energy they absorb from each other would lead to their fluorescence diminishing. This property can also be applied to develop "turn-on" mAb conjugates (Fig. 12D) [101–103]. Since NIR probes are of great interest for in vivo imaging, the self-quenching properties of NIR fluorophores were also investigated. The cyanine-based NIR fluorophore Alexa680 was conjugated to trastuzumab (Tra-Alexa680 (SQ)) and the quenching capacity was 8-fold. In vitro microscopy demonstrated that the fluorescence of SQ was quenched outside the HER2-positive cell, but restored after entering the cell. When the probe was applied in vivo, SQ showed a high tumor-to-background ratio and only the target HER2-positive tumor was fluorescent [104]. One of the key points in designing such self-quenched probes is the close enough distance between fluorophores, but in most cases this is too difficult to control during

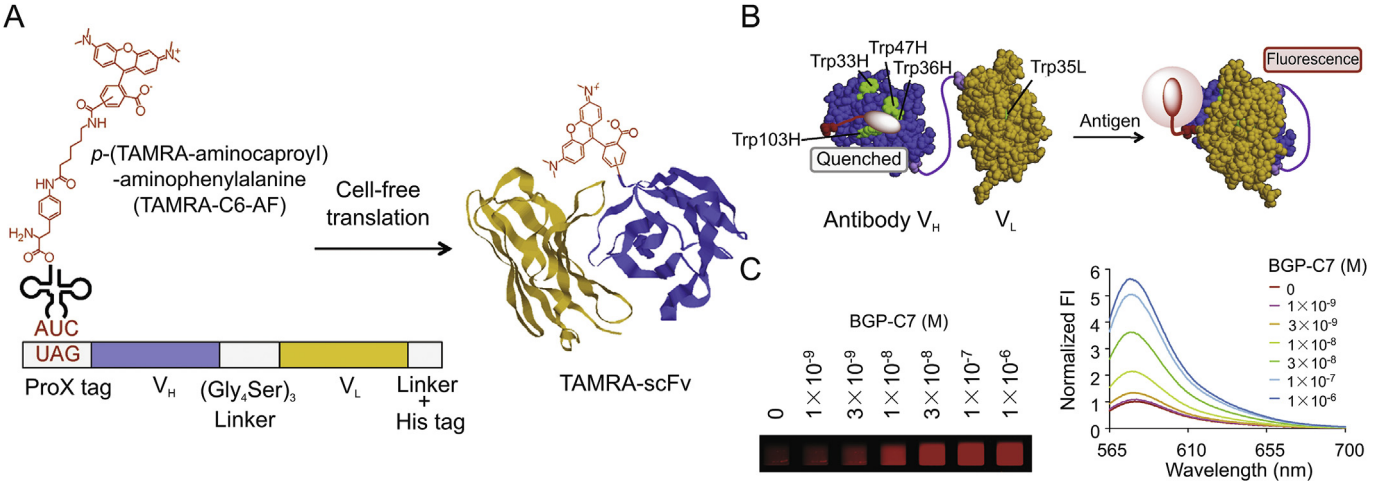

Fig. 15. (A) Incorporation of TAMRA-C6-AF into scFv in response to a UAG codon in a cell-free translation system. (B) The reaction model of TAMRA-scFv towards antigen. Trp residues, Trp33H, Trp36H, Trp47H, Trp103H, and Trp35L are colored green. (C) Antigen-dependent fluorescence enhancement of TAMRA-labeled anti-BGP scFv upon reaction with BGP-C7. The figure was reproduced with permission from Ref. [106].

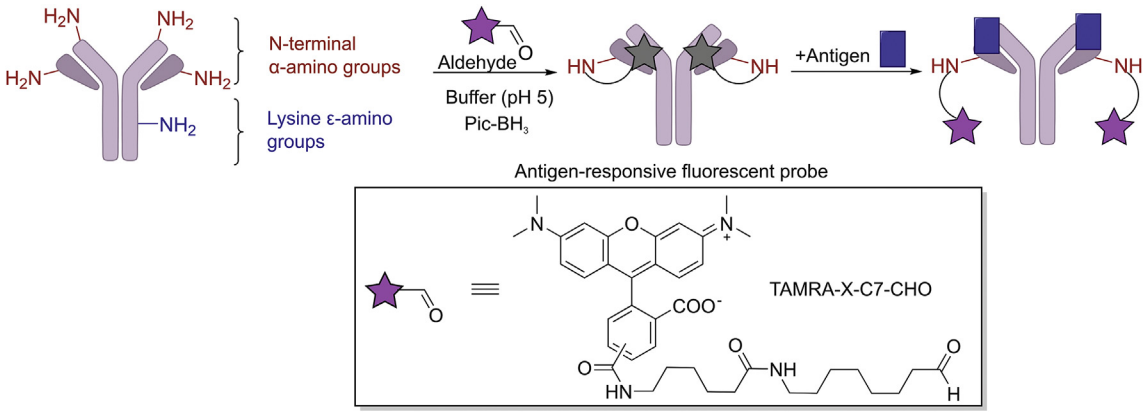

Fig. 16. Schematic illustration of N-terminal selective fluorescent labeling of IgG and fluorescence response upon antigen-binding [108].

the conjugation [105].

3.3.2. *Fluorescence activated upon antigen binding*

The above-mentioned activatable systems showed low non-specific background, but, required a relatively long time to switch on the fluorescence after the receptor-mediated endocytosis and lysosomal degradation of the conjugates, limiting earlier-stage and real-time imaging. Recently, a wash-free antigen-responsive

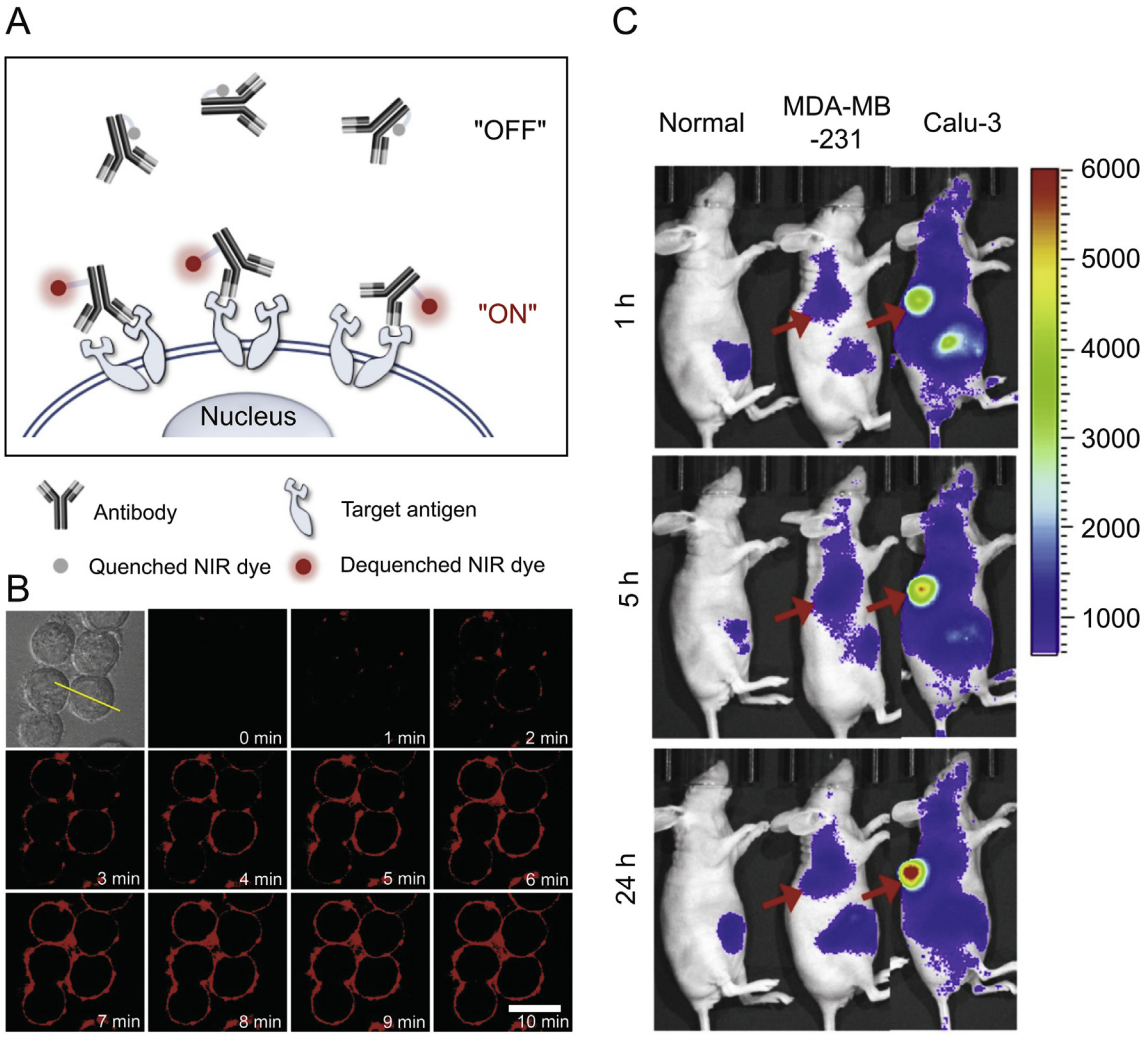

Fig. 17. (A) Diagram of antigen-responsive antibody-NIR fluorophore conjugates for activatable fluorescence imaging. (B) Real-time fluorescence imaging of membrane binding HER-ATTO680 on SK-BR-3 cells acquired every 1 min (λ_{ex} = 633 nm, λ_{em} = 647–754 nm) without washing. (C) In vivo NIR fluorescence images of normal, MDA-MB-231 and Calu-3 tumor-bearing mice upon HER-ATTO680-treatment (λ_{ex} = 660/20 nm, λ_{em} = 710/40 nm). The figure was reproduced with permission from Ref. [109].

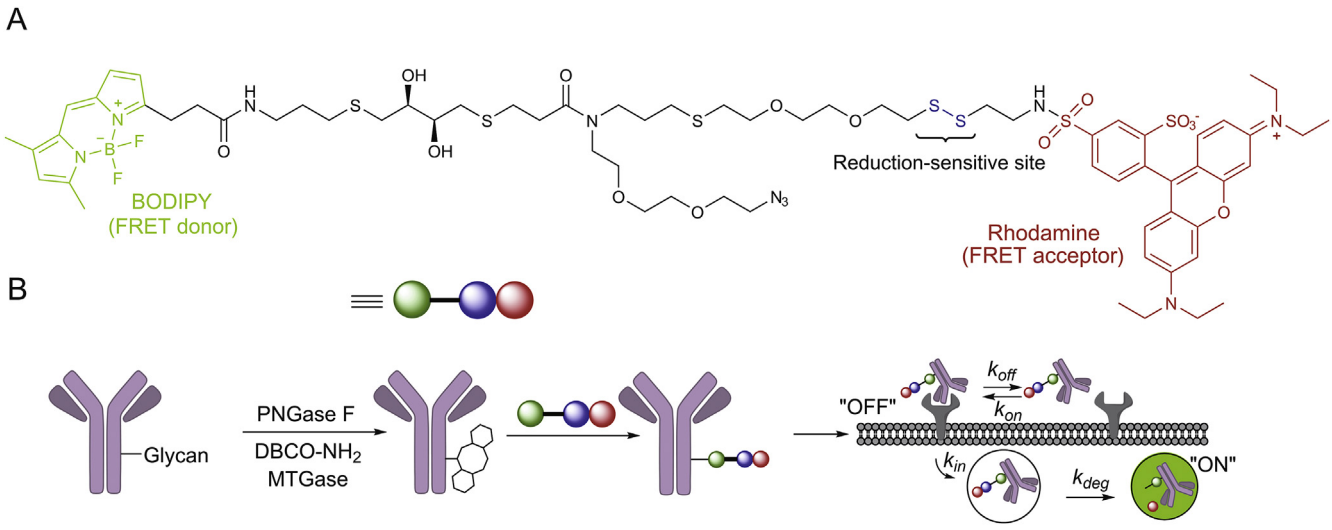

Fig. 18. (A) The chemical structure of the cleavable crosslinker furnished with a FRET fluorophore pair. (B) Schematic of site-specific modification of trastuzumab via microbial transglutaminase and its "turn-on" response after entering cells [110].

detection strategy, also called "quenchbody", has been developed [106,107]. Ueda's group described a novel reagentless fluorescent biosensor based on the antigen-competitive removal of a quenching effect on the fluorophore. The natural amino acid tryptophan (Trp) is known to serve as an efficient electron donor in photoinduced electron transfer (PeT) reactions with certain dyes. Using a position-specific protein labeling methodology, TAMRA-labeled amino acid was incorporated into Anti-BGP scFv (Fig. 15A). TAMRA penetrates between the V_H/V_L interface and interacts with nearby Trp residues by hydrophobic and/or π-π stacking interactions, probably leading to a quenching PeT from the Trp residues to the dye (Fig. 15B). Binding of an antigen, such as the BGP peptide (BGP-C7), to the scFv induces tighter complexation of V_H and V_L, releases the TAMRA dye from interactions with the Trp residues for enhanced emission (Fig. 15C) [106].

To prepare the "quenchbody", an expanded genetic code system (i.e., amber and four-base codons) along with a cell-free translation system needs to be employed. However, the yield of unnatural amino acid-containing proteins is frequently low. Additionally, genetic information of mAbs is needed; however, the information is often unrevealed. To overcome these limitations, Hohsaka's group [108] utilized reductive alkylation under weak acidic pH conditions to selectively label N-terminal of an IgG-type antibody (Fig. 16), which produced antigen-responsive fluorescence (e.g., fluorescein-

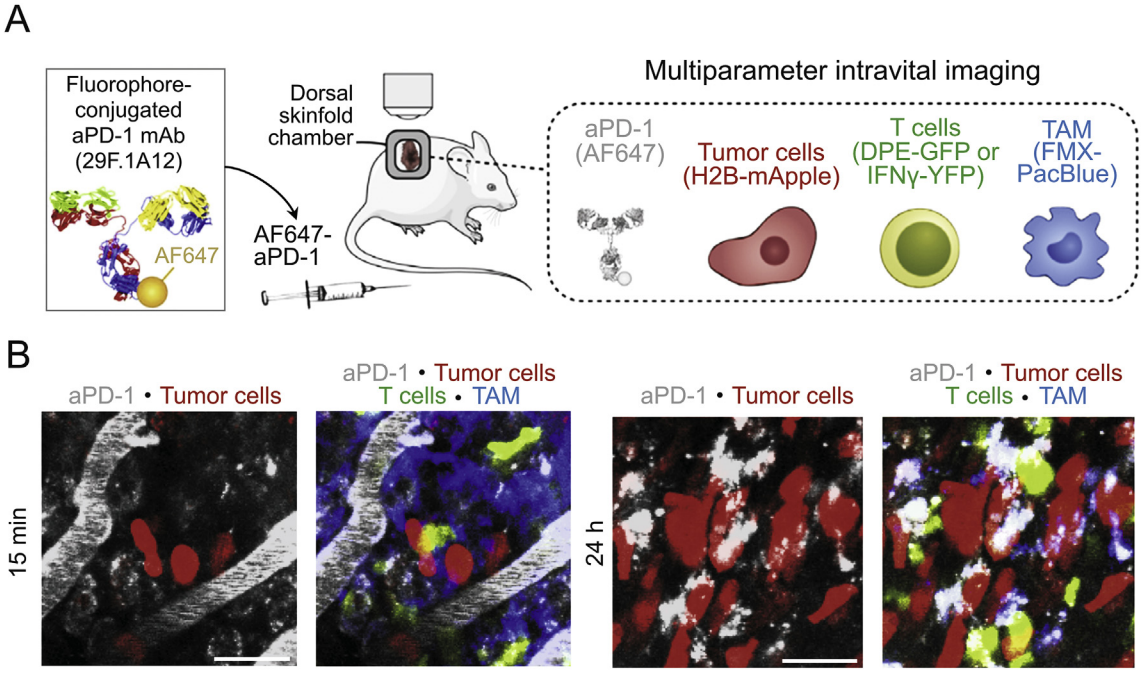

Fig. 19. (A) The rat anti-mouse PD-1 29F.1A12 clone, conjugated to AF647 via NHS ester linkage (left). Diagram depicting intravital imaging setup with labeled aPD-1, MC38 tumor cells, T cells, and TAMs (right). (B) Z-projections of an MC38-H2B-mApple tumor in a DPE-GFP mouse injected intravenously with AF647–aPD-1 after 15 min (left) or 24 h (right). The figure was reproduced with permission from Ref. [111].

labeled anti-FLAG-tag IgG exhibited a fluorescence response of $F/F_0 = 3.3 \pm 0.1$ upon binding to FLAG peptide).

To take one step further, a series of NIR fluorophores, such as Alexa680, ATTO655, ATTO680 and ATTO700, reacted with the lysine (Lys) residues of trastuzumab at various molar ratios to check their feasibility for constructing "quenchbody". Most of these fluorophores underwent fluorescence quenching by tryptophan and/or tyrosine with the PeT mechanism (Fig. 17A). The trastuzumab-ATTO680 conjugate, HER-ATTO680, with 3.77 DL (the degree of labeling) showed the best quenching effect (Fig. 17B/C) [109]. However, such random labeling towards the highly abundant Lys residues is likely to limit the quenching efficiency when applied to other mAbs.

To be noted, the fluorescence change from the latter strategy (section 3.3.2) is highly dependent on the type of mAb because of the difference in local structures around Trp residues. Efforts are still needed to develop "universal" activatable strategies suitable for most mAbs, allowing easy conversion of the commercially available antibodies into turn-on probes for the detection of various antigens according to research interests. More importantly, fluorescent antibody conjugates described here with the "turn-on" property have also been widely adopted for early cancer diagnosis and fluorescence-guided surgery to visualize tumor margins with improved accuracy, encouraging the development of such no-wash imaging designs.

3.3.3. ADC cleavage

In addition to functioning alone for therapeutic purposes, immunoconjugates such as ADCs containing cytotoxic payloads through a chemical crosslinker also have entered the drug market (Fig. 2). The cleavable bond incorporated into the crosslinker is often the key to achieving spatiotemporally controllable release of drug payload inside the target cell. To quantitatively study the cleavage of specific chemical bonds from the mAb, Alabi's group conjugated a FRET donor and the paired acceptor to each side of the crosslinker to visualize the fluorescence change (Fig. 18A). After entering cells upon endocytosis, the conjugate got cleaved under the reducing environment and exhibited the fluorescence change from red to green through FRET (Fig. 18B) [110], indicating the intracellular processing and assessing the amount of released payload inside the cell.

3.4. Antibody-effector cell interaction

Another key attribute of mAbs is their ability to recruit or block other effector cells (such as natural killer (NK) cells, T cells and macrophages) to mediate the cell fate (Fig. 2). The recruitment is mainly mediated by the Fc of the antibody, which includes the heavy-chain second and third constant regions (Fig. 1A).

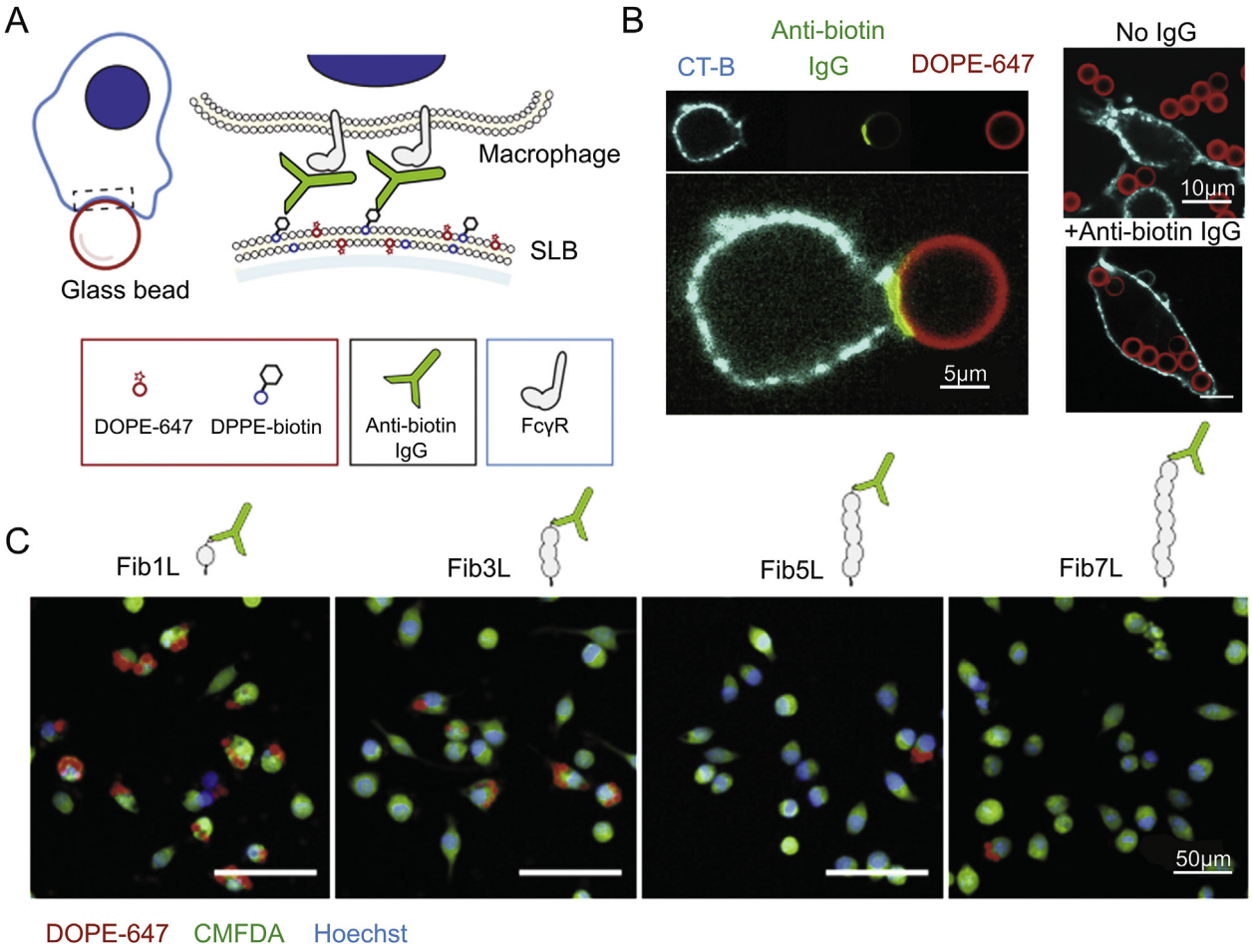

Fig. 20. (A) Target glass beads were coated by a lipid bilayer (containing DPPE-biotin, labeled by DOPE-647 in red). Anti-biotin IgG binds to the lipid surface through interaction with the biotin group of DPPE-biotin. Binding between FcγRs on the macrophage surface and the Fc region of anti-biotin IgG is shown. (B) Left: confocal imaging of a RAW 264.7 macrophage-like cell (membrane is labeled with cholera-toxin B 555, cyan) at a contact interface with a target bead in the presence of anti-biotin IgG (labeled with Alexa Fluor 488, green). Right: target beads containing only lipids (up) or pre-incubated with anti-biotin IgG (down) were added to RAW 264.7 cells. (C) Confocal imaging of phagocytosis of target beads bound with biotinylated Fib1L, Fib3L, Fib5L, and Fib7L protein antigens and opsonized with anti-biotin IgG. Cells were labeled with 0.5 μM CellTracker Green (CMFDA) and Hoechst. The figure was reproduced with permission from Ref. [112].

Currently approved immune checkpoint blockers are mAbs that target the programmed cell death protein 1 (PD-1) or cytotoxic T lymphocyte-associated protein 4 pathways, and agents targeting other pathways are in clinical development (including OX40, Tim-3, and LAG-3). They have demonstrated impressive benefits for the treatment of some cancers; however, these drugs are not always effective, and we still have a limited understanding of the mechanisms that contribute to their efficacy or resistance. Much less is known about their interactions with host components in the tumor bed.

Arlauckas et al. used intravital imaging to follow fluorescently labeled anti-PD-1 mAb (aPD-1) in real time and at subcellular resolution to uncover the fate and activity of aPD-1 in mice. They focused on aPD-1 interactions with various effector cells by simultaneously assessing aPD-1 (labeled with AlexaFluor647, AF647-aPD-1), MC38 tumor cells (labeled with H2B-mApple), T cells (labeled with green fluorescent protein (GFP) or yellow fluorescent protein (YFP)), and tumor-associated macrophages (TAMs, labeled with Pacific Blue-dextran nanoparticles; Fig. 19A). By using time lapse intravital microscopy, they uncovered in real time how aPD-1 distributes in tumors and physically interacts with tumor microenvironment components (Fig. 19B) [111]. Their results showed that aPD-1 initially bound PD-1$^+$ tumor-infiltrating CD8$^+$ T cells (Fig. 19B left), but could then be quickly captured from the T cell surface by PD-1$^-$ tumor-associated macrophages (Fig. 19B right), which may limit the therapeutic efficacy. Further study showed that macrophage accrual of aPD-1 depends both on the drug's Fc domain glycan and on Fcγ receptors (FcγRs) expressed by host myeloid cells [111].

Different from the above immune checkpoint blockers, where the interaction of mAbs with tumor associated macrophages decrease their efficacy, other cancer cell-targeting mAbs recruit effector cells to enhance the anti-tumor immunity. In a recent study, the antibody-dependent cellular phagocytosis (ADCP) in cancer immunotherapy using mAbs was investigated upon live-cell imaging [112]. Using a reconstituted model of antibody-opsonized target cells (Fig. 20A), they observed a significant enrichment of labeled anti-biotin IgG in RAW264.7 macrophage-like cells (Fig. 20B). Strikingly, decreasing phagocytosis was seen with increasing antigen height when using biotinylated Fib1L, Fib3L, Fib5L, and Fib7L protein antigens (n in FibnL represents the repeats of a synthetic FNIII domain, Fibcon, which is to model antigens of different heights; Fig. 20C) and suggested that phagocytosis is dramatically impaired for antigens that position antibodies >10 nm from the target surface. These findings indicate that the multi-color live-cell imaging helps to uncover fundamental aspects of the interaction between mAb and effector cells in real time, providing insights to further improve the outcome of antibody therapy.

4. Perspectives

Consistent efforts made in the area of pharmaceutical analysis have facilitated the quality control and pharmacokinetic studies of macromolecular drugs like therapeutic monoclonal antibodies. In view of the increasingly important role of mAbs in the treatment and prevention of various diseases along with the continuous supply of innovative mAb products in the future, there should be concomitant rise in the development of companion detection and analysis methods towards mAbs and their derivatives.

Specially, functional assessment at molecular level remains challenging due to a lack of practical strategies and tools that can characterize mAb-based candidates during preclinical and clinical studies. Molecular imaging holds a great potential as a noninvasive visualization of biological processes at the molecular level within intact living organisms [113,114]. Among which, PET is promising for measuring target engagement of mAbs to predict toxicity and efficacy, which has also shown capability for clinical translation [115]. However, PET suffers from insufficient spatial resolution and expensive cost. Fluorescence imaging has grown significantly over the past decade as a more cost-efficient real-time imaging modality. To reduce the background of non-specific signals, activatable mAb-fluorophore conjugates are preferred for no-wash imaging of dynamic cell response upon mAb treatment, while the development is still in its infancy. To make fluorescence imaging a standard practice, more "turn-on" imaging reagents need to be accessible in the future, offering opportunities to identify the diseases at an early stage [116–118] and being adopted to guide tumor resection in clinic to fight against the diseases more efficiently. Furthermore, quantitation with fluorescence imaging should be guaranteed with new techniques/strategies to better interpret the intravital efficacy of mAbs. And more attention should also be paid to the fate of mAbs after administration, including long-term dynamics of mAb like its internalization, degradation, and recycling processes, as well as to achieving multi-color imaging towards microenvironment factors that may interfere mAbs.

After obtaining more imperative information regarding the biological functions of mAbs and their associated microenvironment in vivo, this novel knowledge can be utilized for both improving the understanding of cancer and furthering our exploration of new therapeutic mAbs. Improvements in disease models [119] like patient derived xenografts [120], 3D printed cancer model [121] and microfluidic systems [122,123] mimicking the real disease conditions can indeed assist these studies.

Declaration of competing interest

The authors declare that there are no conflicts of interest.

Acknowledgments

We acknowledge financial support from the National Natural Science Foundation of China (81903574) and the Fundamental Research Funds for the Central Universities (2019QNA7046; 2020QNA7001).

References

[1] G.J. Weiner, Building better monoclonal antibody-based therapeutics, Nat. Rev. Cancer 15 (2015) 361–370.
[2] P.J. Carter, G.A. Lazar, Next generation antibody drugs: pursuit of the 'high-hanging fruit', Nat. Rev. Drug Discov. 17 (2018) 197–223.
[3] K. Tsumoto, Y. Isozaki, H. Yagami, et al., Future perspectives of therapeutic monoclonal antibodies, Immunotherapy 11 (2019) 119–127.
[4] G. Köhler, C. Milstein, Continuous cultures of fused cells secreting antibody of predefined specificity, Nature 256 (1975) 495–497.
[5] K.R. Rodgers, R.C. Chou, Therapeutic monoclonal antibodies and derivatives: historical perspectives and future directions, Biotechnol. Adv. 34 (2016) 1149–1158.
[6] H. Kaplon, M. Muralidharan, Z. Schneider, et al., Antibodies to watch in 2020, mAbs 12 (2020), 1703531.
[7] X. Wang, Z.Q. An, W.X. Luo, et al., Molecular and functional analysis of monoclonal antibodies in support of biologics development, Protein Cell 9 (2018) 74–85.
[8] S. Rosati, Y. Yang, A. Barendregt, et al., Detailed mass analysis of structural heterogeneity in monoclonal antibodies using native mass spectrometry, Nat. Protoc. 9 (2014) 967–976.
[9] Y.T. Jin, Z.Q. Lin, Q.G. Xu, et al., Comprehensive characterization of monoclonal antibody by Fourier transform ion cyclotron resonance mass spectrometry, mAbs 11 (2019) 106–115.
[10] O. Heudi, S. Barteau, D. Zimmer, et al., Towards absolute quantification of therapeutic monoclonal antibody in serum by LC-MS/MS using isotope-labeled antibody standard and protein cleavage isotope dilution mass spectrometry, Anal. Chem. 80 (2008) 4200–4207.
[11] A. Martinez-Ortega, A. Herrera, A. Salmeron-Garcia, et al., Study and ICH validation of a reverse-phase liquid chromatographic method for the

quantification of the intact monoclonal antibody cetuximab, J. Pharm. Anal. 6 (2016) 117–124.
[12] M. Haberger, M. Leiss, A.K. Heidenreich, et al., Rapid characterization of biotherapeutic proteins by size-exclusion chromatography coupled to native mass spectrometry, mAbs 8 (2016) 331–339.
[13] A. Ehkirch, A. Goyon, O. Hernandez-Alba, et al., A novel online four-dimensional SECxSEC-IMxMS methodology for characterization of monoclonal antibody size variants, Anal. Chem. 90 (2018) 13929–13937.
[14] F. Füssl, K. Cook, K. Scheffler, et al., Charge variant analysis of monoclonal antibodies using direct coupled pH gradient cation exchange chromatography to high-resolution native mass spectrometry, Anal. Chem. 90 (2018) 4669–4676.
[15] M. Han, B.M. Rock, J.T. Pearson, et al., Intact mass analysis of monoclonal antibodies by capillary electrophoresis-mass spectrometry, J. Chromatogr. B 1011 (2016) 24–32.
[16] L.C. Zhang, A.M. English, D.L. Bai, et al., Analysis of monoclonal antibody sequence and post-translational modifications by time-controlled proteolysis and tandem mass spectrometry, Mol. Cell. Proteomics 15 (2016) 1479–1488.
[17] H. Yang, S. Yang, J. Kong, et al., Obtaining information about protein secondary structures in aqueous solution using Fourier transform IR spectroscopy, Nat. Protoc. 10 (2015) 382–396.
[18] A. Micsonai, F. Wien, L. Kernya, et al., Accurate secondary structure prediction and fold recognition for circular dichroism spectroscopy, Proc. Natl. Acad. Sci. U.S.A. 112 (2015) E3095–E3103.
[19] D. Tsuchida, K. Yamazaki, S. Akashi, Comprehensive characterization of relationship between higher-order structure and FcRn binding affinity of stress-exposed monoclonal antibodies, Pharm. Res. (N. Y.) 33 (2016) 994–1002.
[20] R.Y.-C. Huang, G. Chen, Higher order structure characterization of protein therapeutics by hydrogen/deuterium exchange mass spectrometry, Anal. Bioanal. Chem. 406 (2014) 6541–6558.
[21] Y. Song, D. Yu, M. Mayani, et al., Monoclonal antibody higher order structure analysis by high throughput protein conformational array, mAbs 10 (2018) 397–405.
[22] J.N. Arnold, M.R. Wormald, R.B. Sim, et al., The impact of glycosylation on the biological function and structure of human immunoglobulins, Annu. Rev. Immunol. 25 (2007) 21–50.
[23] A. Beck, E. Wagner-Rousset, D. Ayoub, et al., Characterization of therapeutic antibodies and related products, Anal. Chem. 85 (2013) 715–736.
[24] H.H. Shi, C.T. Goudar, Recent advances in the understanding of biological implications and modulation methodologies of monoclonal antibody N-linked high mannose glycans, Biotechnol. Bioeng. 111 (2014) 1907–1919.
[25] G. Vidarsson, G. Dekkers, T. Rispens, IgG subclasses and allotypes: from structure to effector functions, Front. Immunol. 5 (2014) 520.
[26] F. Higel, A. Seidl, F. Sorgel, et al., N-glycosylation heterogeneity and the influence on structure, function and pharmacokinetics of monoclonal antibodies and Fc fusion proteins, Eur. J. Pharm. Biopharm. 100 (2016) 94–100.
[27] F. Cymer, H. Beck, A. Rohde, et al., Therapeutic monoclonal antibody N-glycosylation structure, function and therapeutic potential, Biologicals 52 (2018) 1–11.
[28] K.J. Arlotta, S.C. Owen, Antibody and antibody derivatives as cancer therapeutics, WIREs Nanomed. Nanobi. 11 (2019) e1556.
[29] A. Beck, E. Wagner-Rousset, M.C. Bussat, et al., Trends in glycosylation, glycoanalysis and glycoengineering of therapeutic antibodies and Fc-fusion proteins, Curr. Pharmaceut. Biotechnol. 9 (2008) 482–501.
[30] M.X. Sliwkowski, I. Mellman, Antibody therapeutics in cancer, Science 341 (2013) 1192–1198.
[31] C. Li, L.X. Wang, Chemoenzymatic methods for the synthesis of glycoproteins, Chem. Rev. 118 (2018) 8359–8413.
[32] M.M. Chang, L. Gaidukov, Y. Jung, et al., Small-molecule control of antibody N-glycosylation in engineered mammalian cells, Nat. Chem. Biol. 15 (2019) 730–736.
[33] S. Ha, Y. Wang, R.R. Rustandi, Biochemical and biophysical characterization of humanized IgG1 produced in Pichia pastoris, mAbs 3 (2011) 453–460.
[34] M. Tanaka, A. Koga, A. Kobe, et al., O-linked glucosylation of a therapeutic recombinant humanised monoclonal antibody produced in CHO cells, Eur. J. Pharm. Biopharm. 83 (2013) 123–130.
[35] Z.Q. Zhang, H. Pan, X.Y. Chen, Mass spectrometry for structural characterization of therapeutic antibodies, Mass Spectrom. Rev. 28 (2009) 147–176.
[36] S. Carillo, R. Pérez-Robles, C. Jakes, et al., Comparing different domains of analysis for the characterisation of N-glycans on monoclonal antibodies, J. Pharm. Anal. 10 (2020) 23–34.
[37] R.R. Rustandi, M.W. Washabaugh, Y. Wang, Applications of CE SDS gel in development of biopharmaceutical antibody-based products, Electrophoresis 29 (2008) 3612–3620.
[38] M. Biacchi, R. Gahoual, N. Said, et al., Glycoform separation and characterization of cetuximab variants by middle-up off-line capillary zone electrophoresis-UV/electrospray ionization-MS, Anal. Chem. 87 (2015) 6240–6250.
[39] G. Lu, C.L. Crihfield, S. Gattu, et al., Capillary electrophoresis separations of glycans, Chem. Rev. 118 (2018) 7867–7885.
[40] A.M. Scott, J.D. Wolchok, L.J. Old, Antibody therapy of cancer, Nat. Rev. Cancer 12 (2012) 278–287.
[41] N.W.C.J. van de Donk, P. Moreau, T. Plesner, et al., Clinical efficacy and management of monoclonal antibodies targeting CD38 and SLAMF7 in multiple myeloma, Blood 127 (2016) 681–695.
[42] E. Cruz, V. Kayser, Monoclonal antibody therapy of solid tumors: clinical limitations and novel strategies to enhance treatment efficacy, Biol. Targets & Ther. 13 (2019) 33–51.
[43] A. Young, Z. Quandt, J.A. Bluestone, The balancing act between cancer immunity and autoimmunity in response to immunotherapy, Cancer Immunol. Res. 6 (2018) 1445–1452.
[44] J.T. Ryman, B. Meibohm, Pharmacokinetics of monoclonal antibodies, CPT Pharmacometrics Syst. Pharmacol. 6 (2017) 576–588.
[45] J.H.E. Baker, A.H. Kyle, S.A. Reinsberg, et al., Heterogeneous distribution of trastuzumab in HER2-positive xenografts and metastases: role of the tumor microenvironment, Clin. Exp. Metastasis 35 (2018) 691–705.
[46] J. Davda, P. Declerck, S. Hu-Lieskovan, et al., Immunogenicity of immunomodulatory, antibody-based, oncology therapeutics, J. Immunother. Cancer 7 (2019) 105.
[47] Y.T. Cong, Z. Zhang, S. Zhang, et al., Quantitative MS analysis of therapeutic mAbs and their glycosylation for pharmacokinetics study, Proteonomics Clin. Appl. 10 (2016) 303–314.
[48] D. Ternant, T. Lecomte, D. Degenne, et al., An enzyme-linked immunosorbent assay to study bevacizumab pharmacokinetics, Ther. Drug Monit. 32 (2010) 647–652.
[49] M. Aoyama, Y. Mano, Application of an electrochemiluminescence assay for quantification of E6011, an antifractalkine monoclonal antibody, to pharmacokinetic studies in monkeys and humans, J. Clin. Lab. Anal. 33 (2019), e22625.
[50] Y. Zhang, R. Zhang, X. Yang, et al., Recent advances in electrogenerated chemiluminescence biosensing methods for pharmaceuticals, J. Pharm. Anal. 9 (2019) 9–19.
[51] Y. Dai, C.C. Liu, Recent advances on electrochemical biosensing strategies toward universal point-of-care systems, Angew. Chem. Int. Ed. Engl. 58 (2019) 12355–12368.
[52] R.J. White, H.M. Kallewaard, W. Hsieh, et al., Wash-free, electrochemical platform for the quantitative, multiplexed detection of specific antibodies, Anal. Chem. 84 (2012) 1098–1103.
[53] J.D. Lu, T. Van Stappen, D. Spasic, et al., Fiber optic-SPR platform for fast and sensitive infliximab detection in serum of inflammatory bowel disease patients, Biosens. Bioelectron. 79 (2016) 173–179.
[54] M. Beeg, A. Nobili, B. Orsini, et al., A surface plasmon resonance-based assay to measure serum concentrations of therapeutic antibodies and anti-drug antibodies, Sci. Rep. 9 (2019) 2064.
[55] M. van Rosmalen, Y. Ni, D.F.M. Vervoort, et al., Dual-color bioluminescent sensor proteins for therapeutic drug monitoring of antitumor antibodies, Anal. Chem. 90 (2018) 3592–3599.
[56] X. Liu, J.K. Lukowski, C. Flinders, et al., MALDI-MSI of immunotherapy: mapping the EGFR-targeting antibody cetuximab in 3D colon-cancer cell cultures, Anal. Chem. 90 (2018) 14156–14164.
[57] A.R. Tan, J.K. Lukowski, C. Flinders, et al., Pharmacokinetics of cetuximab after administration of escalating single dosing and weekly fixed dosing in patients with solid tumors, Clin. Cancer Res. 12 (2006) 6517–6522.
[58] F. Becher, J. Ciccolini, D.C. Imbs, et al., A simple and rapid LC-MS/MS method for therapeutic drug monitoring of cetuximab: a GPCO-UNICANCER proof of concept study in head-and-neck cancer patients, Sci. Rep. 7 (2017) 2714.
[59] K. Chen, X.Y. Chen, Positron emission tomography imaging of cancer biology: current status and future prospects, Semin. Oncol. 38 (2011) 70–86.
[60] C.W. Menke-van der Houven van Oordt, E.C. Gootjes, M.C. Huisman, et al., ^{89}Zr-cetuximab PET imaging in patients with advanced colorectal cancer, Oncotarget 6 (2015) 30384–30393.
[61] G. Niu, Z.B. Li, J. Xie, et al., PET of EGFR antibody distribution in head and neck squamous cell carcinoma models, J. Nucl. Med. 50 (2009) 1116–1123.
[62] Y.-H. Xie, Y.-X. Chen, J.-Y. Fang, Comprehensive review of targeted therapy for colorectal cancer, Signal Transduct. Tar. 5 (2020) 22.
[63] A. Yamaguchi, A. Achmad, H. Hanaoka, et al., Immuno-PET imaging for non-invasive assessment of cetuximab accumulation in non-small cell lung cancer, BMC Cancer 19 (2019) 1000.
[64] A.N. Niemeijer, D. Leung, M.C. Huisman, et al., Whole body PD-1 and PD-L1 positron emission tomography in patients with non-small-cell lung cancer, Nat. Commun. 9 (2018) 4664.
[65] S. Heskamp, R. Raave, O. Boerman, et al., ^{89}Zr-Immuno-positron emission tomography in oncology: state-of the-art ^{89}Zr radiochemistry, Bioconjugate Chem. 28 (2017) 2211–2223.
[66] C.A. Foss, L. Kulik, A.A. Ordonez, et al., SPECT/CT imaging of mycobacterium tuberculosis infection with [^{125}I]anti-C3d mAb, Mol. Imag. Biol. 21 (2019) 473–481.
[67] M. Patra, L.S. Eichenberger, G. Fischer, et al., Photochemical conjugation and one-pot radiolabelling of antibodies for Immuno-PET, Angew. Chem. Int. Ed. Engl. 58 (2019) 1928–1933.
[68] M. Morais, M.T. Ma, Site-specific chelator-antibody conjugation for PET and SPECT imaging with radiometals, Drug Discov. Today Technol. 30 (2018) 91–104.
[69] P. Adumeau, S.K. Sharma, C. Brent, et al., Site-specifically labeled immunoconjugates for molecular imaging-Part 1: cysteine residues and glycans, Mol. Imag. Biol. 18 (2016) 1–17.
[70] D. Vivier, K. Fung, C. Rodriguez, et al., The influence of glycans-specific bioconjugation on the FcγRI binding and in vivo performance of ^{89}Zr-DFO-pertuzumab, Theranostics 10 (2020) 1746–1757.

[71] L. Qian, J. Fu, P. Yuan, et al., Intracellular delivery of native proteins facilitated by cell-penetrating poly(disulfide)s, Angew. Chem. Int. Ed. Engl. 57 (2018) 1532–1536.
[72] E. Berg, H. Gill, J. Marik, et al., Total-body PET and highly stable chelators together enable meaningful ^{89}Zr-antibody-PET studies up to 30 days after injection, J. Nucl. Med. 61 (2020) 453–460.
[73] M.A. Pysz, S.S. Gambhir, J.K. Willmann, Molecular imaging: current status and emerging strategies, Clin. Radiol. 65 (2010) 500–516.
[74] M. Goetz, M.S. Hoetker, M. Diken, P.R. Galle, R. Kiesslich, In vivo molecular imaging with cetuximab, an anti-EGFR antibody, for prediction of response in xenograft models of human colorectal cancer, Endoscopy 45 (2013) 469–477.
[75] C. Cilliers, I. Nessler, N. Christodolu, et al., Tracking antibody distribution with near-infrared fluorescent dyes: impact of dye structure and degree of labeling on plasma clearance, Mol. Pharm. 14 (2017) 1623–1633.
[76] W. Bernhard, A. El-Sayed, K. Barreto, et al., Near infrared fluorescence imaging of EGFR expression in vivo using IRDye800CW-nimotuzumab, Oncotarget 9 (2018) 6213–6227.
[77] Y. Hama, Y. Koyama, Y. Urano, et al., Two-color lymphatic mapping using Ig-conjugated near infrared optical probes, J. Invest. Dermatol. 127 (2007) 2351–2356.
[78] Y. Koyama, T. Barrett, Y. Hama, et al., In vivo molecular imaging to diagnose and subtype tumors through receptor-targeted optically labeled monoclonal antibodies, Neoplasia 9 (2007) 1021–1029.
[79] H. Kobayashi, M.R. Longmire, M. Ogawa, et al., Rational chemical design of the next generation of molecular imaging probes based on physics and biology: mixing modalities, colors and signals, Chem. Soc. Rev. 40 (2011) 4626–4648.
[80] K. Sano, M. Mitsunaga, T. Nakajima, et al., In vivo breast cancer characterization imaging using two monoclonal antibodies activatably labeled with near infrared fluorophores, Breast Cancer Res. 14 (2012) R61.
[81] M. Longmire, N. Kosaka, M. Ogawa, et al., Multicolor in vivo targeted imaging to guide real-time surgery of HER2-positive micrometastases in a two-tumor coincident model of ovarian cancer, Cancer Sci. 100 (2009) 1099–1104.
[82] S.H. Ahn, D. Thach, B. Vaughn, et al., Linear Desferrichrome-linked silicon-rhodamine antibody conjugate enables targeted multimodal imaging of HER2 in vitro and in vivo, Mol. Pharm. 16 (2019) 1412–1420.
[83] Y.W.S. Jauw, J.A. O'Donoghue, J.M. Zijlstra, et al., ^{89}Zr-Immuno-PET: toward a noninvasive clinical tool to measure target engagement of therapeutic antibodies in vivo, J. Nucl. Med. 60 (2019) 1825–1832.
[84] L. Heinrich, N. Tissot, D.J. Hartmann, et al., Comparison of the results obtained by ELISA and surface plasmon resonance for the determination of antibody affinity, J. Immunol. Methods 352 (2010) 13–22.
[85] J.A. Maynard, N.C. Lindquist, J.N. Sutherland, et al., Surface plasmon resonance for high-throughput ligand screening of membrane-bound proteins, Biotechnol. J. 4 (2009) 1542–1558.
[86] W. Ma, L. Yang, L. He, Overview of the detection methods for equilibrium dissociation constant K_D of drug-receptor interaction, J. Pharm. Anal. 8 (2018) 147–152.
[87] J. Qin, X. Li, L. Cao, et al., Competition-based universal photonic crystal biosensors by using antibody-antigen interaction, J. Am. Chem. Soc. 142 (2020) 417–423.
[88] D.H. Kim, K. Zhou, D.K. Kim, et al., Analysis of interactions between the epidermal growth factor receptor and soluble ligands on the basis of single-molecule diffusivity in the membrane of living cells, Angew. Chem. Int. Ed. Engl. 54 (2015) 7028–7032.
[89] Q.R. Zhang, Y. Shi, H.J. Xu, et al., Evaluating the efficacy of the anticancer drug cetuximab by atomic force microscopy, RSC Adv. 8 (2018) 21793–21797.
[90] Y. Tang, K. Parag-Sharma, A.L. Amelio, et al., A bioluminescence resonance energy transfer-based approach for determining antibody-receptor occupancy in vivo, iScience 15 (2019) 439–451.
[91] Y. Li, P.C. Liu, Y. Shen, et al., A cell-based internalization and degradation assay with an activatable fluorescence-quencher probe as a tool for functional antibody screening, J. Biomol. Screen 20 (2015) 869–875.
[92] G. Obaid, B.Q. Spring, S. Bano, et al., Activatable clinical fluorophore-quencher antibody pairs as dual molecular probes for the enhanced specificity of image-guided surgery, J. Biomed. Optic. 22 (2017) 1–6.
[93] Y. Urano, D. Asanuma, Y. Hama, et al., Selective molecular imaging of viable cancer cells with pH-activatable fluorescence probes, Nat. Med. 15 (2009) 104–109.
[94] H. Lee, W. Akers, K. Bhushan, et al., Near-infrared pH-activatable fluorescent probes for imaging primary and metastatic breast tumors, Bioconjugate Chem. 22 (2011) 777–784.
[95] J. Mei, N.L. Leung, R.T. Kwok, et al., Aggregation-induced emission: together we shine, united we soar!, Chem. Rev. 115 (2015) 11718–11940.
[96] K. Kokado, K. Sada, Consideration of molecular structure in the excited state to design new luminogens with aggregation-induced emission, Angew. Chem. Int. Ed. Engl. 58 (2019) 8632–8639.
[97] S.D. Xu, Y.K. Duan, B. Liu, Precise molecular design for high-performance luminogens with aggregation-induced emission, Adv. Mater. 32 (2020) e1903530.
[98] X.J. Shi, C.Y.Y. Yu, H.F. Su, et al., A red-emissive antibody-AIEgen conjugate for turn-on and wash-free imaging of specific cancer cells, Chem. Sci. 8 (2017) 7014–7024.
[99] Z. Zhao, X.Y. Zheng, L.L. Du, et al., Non-aromatic annulene-based aggregation-induced emission system via aromaticity reversal process, Nat. Commun. 10 (2019) 2952.
[100] Y.J. Tu, J.K. Liu, H.K. Zhang, et al., Restriction of access to the dark state: a new mechanistic model for heteroatom-containing AIE systems, Angew. Chem. Int. Ed. Engl. 58 (2019) 14911–14914.
[101] M. Ogawa, N. Kosaka, P.L. Choyke, et al., H-Type dimer formation of fluorophores: a mechanism for activatable, in vivo optical molecular imaging, ACS Chem. Biol. 4 (2009) 535–546.
[102] M. Ogawa, N. Kosaka, C.A.S. Regino, et al., High sensitivity detection of cancer in vivo using a dual-controlled activation fluorescent imaging probe based on H-dimer formation and pH activation, Mol. Biosyst. 6 (2010) 888–893.
[103] H. Kobayashi, M. Ogawa, R. Alford, et al., New strategies for fluorescent probe design in medical diagnostic imaging, Chem. Rev. 110 (2010) 2620–2640.
[104] M. Ogawa, C.A.S. Regino, P.L. Choyke, et al., In vivo target-specific activatable near-infrared optical labeling of humanized monoclonal antibodies, Mol. Cancer Ther. 8 (2009) 232–239.
[105] Y.J. Ko, W.J. Kim, K. Kim, et al., Advances in the strategies for designing receptor-targeted molecular imaging probes for cancer research, J. Contr. Release 305 (2019) 1–17.
[106] R. Abe, H. Ohashi, I. Iijima, et al., Quenchbodies": quench-based antibody probes that show antigen-dependent fluorescence, J. Am. Chem. Soc. 133 (2011) 17386–17394.
[107] H. Ueda, J.H. Dong, From fluorescence polarization to quenchbody: recent progress in fluorescent reagentless biosensors based on antibody and other binding proteins, BBA-Proteins Proteom. 1844 (2014) 1951–1959.
[108] K. Fukunaga, T. Watanabe, D. Novitasari, et al., Antigen-responsive fluorescent antibody probes generated by selective N-terminal modification of IgGs, Chem. Commun. 54 (2018) 12734–12737.
[109] H. Kim, H.S. Choi, S.K. Kim, et al., Antigen-responsive molecular sensor enables real-time tumor-specific imaging, Theranostics 7 (2017) 952–961.
[110] M.R. Sorkin, J.A. Walker, S.R. Kabaria, et al., Responsive antibody conjugates enable quantitative determination of intracellular bond degradation rate, Cell Chem. Biol. 26 (2019) 1643–1651.
[111] S.P. Arlauckas, C.S. Garris, R.H. Kohler, et al., In vivo imaging reveals a tumor-associated macrophage-mediated resistance pathway in anti-PD-1 therapy, Sci. Transl. Med. 9 (2017), eaal3604.
[112] M.H. Bakalar, A.M. Joffe, E.M. Schmid, et al., Size-dependent segregation controls macrophage phagocytosis of antibody-opsonized targets, Cell 174 (2018) 131–142.
[113] R. Weissleder, U. Mahmood, Molecular imaging, Radiology 219 (2001) 316–333.
[114] S. Kalimuthu, J.H. Jeong, J.M. Oh, et al., Drug discovery by molecular imaging and monitoring therapy response in lymphoma, Int. J. Mol. Sci. 18 (2017) 1639.
[115] C. Xavier, A. Blykers, D. Laoui, et al., Clinical translation of [^{68}Ga]Ga-NOTA-anti-MMR-sdAb for PET/CT imaging of protumorigenic macrophages, Mol. Imag. Biol. 21 (2019) 898–906.
[116] C.G. England, R. Hernandez, S.B.Z. Eddine, et al., Molecular imaging of pancreatic cancer with antibodies, Mol. Pharm. 13 (2016) 8–24.
[117] K.L. Moek, D. Giesen, I.C. Kok, et al., Theranostics using antibodies and antibody-related therapeutics, J. Nucl. Med. 58 (2017) 83S–90S.
[118] N. Dammes, D. Peer, Monoclonal antibody-based molecular imaging strategies and theranostic opportunities, Theranostics 10 (2020) 938–955.
[119] P. Horvath, N. Aulner, M. Bickle, et al., Screening out irrelevant cell-based models of disease, Nat. Rev. Drug Discov. 15 (2016) 751–769.
[120] Y. Lai, X. Wei, S. Lin, et al., Current status and perspectives of patient-derived xenograft models in cancer research, J. Hematol. Oncol. 10 (2017) 106.
[121] A. Shafiee, A. Atala, Printing technologies for medical applications, Trends Mol. Med. 22 (2016) 254–265.
[122] S.N. Bhatia, D.E. Ingber, Microfluidic organs-on-chips, Nat. Biotechnol. 32 (2014) 760–772.
[123] P. Cui, S.C. Wang, Application of microfluidic chip technology in pharmaceutical analysis: a review, J. Pharm. Anal. 9 (2019) 238–247.